

**Polarization Observations of 1720 MHz OH Masers toward the Three
Supernova Remnants W 28, W 44, and IC 443**

M. J. Claussen, D. A. Frail, and W. M. Goss
National Radio Astronomy Observatory, P.O. Box 0, Socorro, New Mexico 87801
and

R. A. Gaume
United States Naval Observatory, 3450 Mass. Ave., Washington, DC 20392

ABSTRACT

We present arcsecond resolution observations from the VLA¹ with full Stokes polarimetry of the ground-state satellite line of the hydroxyl molecule (OH) at 1720.53 MHz (${}^2\Pi_{3/2}, J = \frac{3}{2}, F = 2 \rightarrow 1$) toward three Galactic supernova remnants: W 28, W 44, and IC 443. The total number of individual OH(1720 MHz) “spots” we detect in each of these three remnants is 41, 25 and 6, respectively. The OH(1720 MHz) features appear to lie along the edge of radio continuum emission from the supernova remnants, but are displaced behind the leading edge of the shock as traced by the synchrotron emission. The brightness temperatures of the OH(1720 MHz) emission features range from 2×10^4 to 10^8 K, convincingly demonstrating the maser nature of the OH(1720 MHz) features. We argue that the partially resolved angular diameters that we measure for the masers are neither intrinsic sizes nor scattering disks, but result from a blend of several unresolved maser features near the same velocity. Thus our computed brightness temperatures are lower limits to the true values. The characteristic antisymmetric “S” profile, indicative of Zeeman splitting in the weak-field case, is identified in the Stokes \mathbf{V} spectrum of several of the brighter maser spots. The derived line-of-sight magnetic fields are of order 0.2 mG and are remarkably constant in both direction and in magnitude over regions several parsecs apart. These are the first measurements of post-shock magnetic fields in supernova remnants and demonstrate the importance of magnetic pressure in these molecular shocks. The velocity dispersion of the maser features is typically less than a few km s^{-1} , and except in the special case of W 28, the mean maser velocity is equal to the systemic velocity of the remnant. We suggest that the maximum amplification of the maser transition will occur when the acceleration produced by the shock is transverse to the line of sight. Additional support for this point comes from the location of the masers in IC 443, and molecular observations which allow the shock geometry to be determined. All of our observations are consistent with a model in which the OH(1720 MHz) is collisionally excited by H_2 molecules in the postshock gas heated by a non-dissociative shock. Finally, we end with a discussion of the importance of supernova remnants with OH(1720 MHz) maser emission as promising candidates to conduct high energy searches for the sites of cosmic ray acceleration.

Subject headings: supernova remnants – masers – ISM: magnetic fields – ISM: individual(W 28, W 44, IC 443)

¹The Very Large Array (VLA) is operated by NRAO, a facility of the National Science Foundation operated under cooperative agreement by Associated Universities, Inc.

1. Introduction

Recognition of the importance of the ground-state satellite line of the hydroxyl molecule (OH) at 1720.53 MHz ($^2\Pi_{3/2}, J = \frac{3}{2}, F = 2 \rightarrow 1$) as a powerful tool for studying the interaction of supernova remnants (SNRs) with molecular clouds has been slow in coming. Anomalous OH(1720 MHz) emission toward the SNRs W 28 and W 44 was originally noted by Goss (1968), Ball & Staelin (1968) and Turner (1969). These and follow up observations by Goss & Robinson (1968) showed that the OH(1720 MHz) line in these regions was strong and narrow and did not have accompanying emission at the other ground-state transitions of OH (1612, 1665 and 1667 MHz), which were instead seen in absorption. Following this initial discovery, other authors noted the OH(1720 MHz) line toward W 28, W 44, and IC 443 (e.g., Hardebeck 1971, Haynes & Caswell 1977, DeNoyer 1979, Turner 1982), but little or no investigation was made as to whether the OH(1720 MHz) lines were associated with the supernova remnants, a suggestion that was tentatively made by Goss & Robinson (1968). The first evidence that this may be the case was presented by Frail, Goss, & Slysh (1994a), who observed W 28 at 12" resolution with the VLA. A total of 26 OH(1720 MHz) emission "spots" were found distributed along the edge of the remnant. The compact nature and high brightness temperature ($T_b \sim 4 \times 10^5$ K) of the spots suggested that these were masers. Based on the location of the masers, and the physical properties of the supernova remnant and the adjacent molecular cloud, Frail et al. (1994a) argued that the OH(1720 MHz) masers in W 28 were consistent with a shock excitation model advocated by Elitzur (1976).

This effort has continued in earnest with a large-scale SNR survey for OH(1720 MHz) with the Green Bank 43-m and Parkes 64-m telescopes, and confirmation observations carried out at the VLA and the Australia Telescope Compact Array (Frail et al. 1996, Green et al. 1997). Based on the early success of identifying OH(1720 MHz) emission toward SNRs near the Galactic Center (Yusef-Zadeh, Uchida & Roberts 1995, Yusef-Zadeh et al. 1996) a VLA survey was conducted of a much larger sample (Robinson et al. 1997). In total we have looked for this line from ~ 166 SNRs and OH(1720 MHz) lines have been confirmed from 17 SNRs, for a detection rate of 10%.

Somewhat less effort has been made on the theoretical side. Most of the recent work concerning the excitation of the OH molecule has been for masers in star-forming regions (Cesaroni & Walmsley 1991, Gray, Doel, & Field 1991). Here the strong far infrared (FIR) radiation field from the dust in the HII region virtually assures that the dominant pumping mechanism is radiative not collisional. The only work that specifically explores the excitation of OH(1720 MHz) under the conditions we expect for SNRs is Elitzur (1976). He showed that in order to create a strong ($-\tau \gg 1$) inversion of the 1720 MHz line, collisions of the OH molecule with H_2 had to occur in a range of kinetic temperature and density between $25 \text{ K} \leq T_k \leq 200 \text{ K}$ and $10^3 \text{ cm}^{-3} \leq n_{H_2} \leq 10^5 \text{ cm}^{-3}$, respectively. Pavlakis & Kylafis (1996a, 1996b) have recently re-visited this topic using newer collisional rates between OH and H_2 (Offer, van Hemert & van Dishoeck 1994) and they included a variety of different pumping mechanisms (collisions, FIR field, local and non-local line overlap). Considering only collisions and local line overlap mechanisms over a restricted range of kinetic temperatures ($T_k=100\text{-}200$ K), they find that bright OH(1720 MHz) maser emission

$T_b \simeq 10^9$ K results at densities (within a factor of three) of $n_{\text{H}_2} = 3 \times 10^5 (10^{-5}/f_{\text{OH}}) \text{ cm}^{-3}$, where f_{OH} is the fractional abundance of OH relative to H_2 . Pavlakis & Kylafis (1996a) also note that OH(1720 MHz) is a sensitive indicator of the amount of ortho- H_2 present relative to para- H_2 , with the inversion reaching a maximum when ortho- H_2 dominates. With further modeling of this type it should be possible to infer the physical conditions of the post-shock gas from the OH(1720 MHz) masers alone.

All the observational work to date has been concerned primarily with identifying new examples of SNR's with the OH(1720 MHz) line. The full potential of the OH(1720 MHz) has yet to be utilized. In this paper we present a detailed study of three SNRs: W 28, W 44, and IC 443. Together they constitute the three best examples of SNRs interacting with molecular clouds. Observations of molecular transitions in the millimeter-wavelength regime toward these three SNRs (e.g., Wootten 1977, Pastchenko & Slysh 1974, DeNoyer 1979, Wootten 1981, Dickman et al. 1992) provide convincing evidence that an interaction is taking place. The goal of the observations reported in this paper are (1) to demonstrate that the OH emission regions are indeed masers by measuring the brightness temperature of the OH(1720 MHz) spots at arcsecond resolution, (2) to demonstrate that the polarized emission from the OH(1720 MHz) masers is due to the Zeeman effect and to measure the magnetic field at several locations in the post-shock gas, (3) to infer physical properties of the environment of the molecular cloud/SNR interface based on the models for the maser emission mechanism and other molecular lines, (4) determine the angular sizes of the masers and to establish whether they are intrinsic or due to strong scattering, and (5) to discern the velocity structure of the interface by observing the spatial distribution of different velocity components.

2. Observations

Observations of the 1720 MHz OH line in three supernova remnants, W 28, W 44 and IC 443 were conducted on March 12 and March 17, 1994, using the Very Large Array of the National Radio Astronomy Observatory.² The VLA was in the **A** configuration, so the resolution at $\lambda=18$ cm was about $1''$. Variations in the u, v coverage for observations of the three supernova remnants make the resulting synthesized beam somewhat different. The synthesized beam sizes for each source are given in Table 1 with the major axis (in arcseconds), the minor axis (in arcseconds) and the rotation of the beam from North in a counterclockwise direction (in degrees). The VLA correlator was configured to produce all four parallel- and cross-polarization products, which were processed into the Stokes parameters **I**, **Q**, **U** and **V**. The data were Hanning smoothed on-line to give velocity resolution of 0.53 km s^{-1} . The total bandwidth was 195 kHz, providing a total velocity coverage of 33.5 km s^{-1} . For W 28, three pointing centers and different central

²The National Radio Astronomy Observatory is a facility of the National Science Foundation, operated under a cooperative agreement by Associated Universities, Inc.

velocities were used in order to observe all sources of the 1720 MHz masers as discovered by Frail et al. (1994a). For W 44 and IC 443 only one pointing center for each supernova remnant was required. Table 1 also gives the position of the pointing centers and the central velocities of the observations. The data for each pointing center were calibrated in the standard manner, including polarization calibration. Images were produced by natural weighting of the u,v data, and were CLEANed in order to remove the effects of the incomplete u,v coverage. For some pointings, multiple fields within the primary beam of the antenna were imaged and cleaned. Images were made in all four Stokes parameters. The rms noise per spectral channel obtained for each object is summarized in the final column of Table 1.

After the imaging step, individual maser features were identified. This was done by carefully examining each spectral channel image individually, and then using the AIPS tasks **JMFIT** and **SAD** to fit the positions of emission features. The positions resulting from using these two tasks were compared and found to agree within the estimated fitting errors (which, for features of typical strength, are about 0.01 times the synthesized beam). For weak features (< 100 mJy beam⁻¹) the fitting errors are somewhat larger, up to 0.1 times the synthesized beam. Positions of individual features were measured from each spectral channel where emission was noted. Gaussians were fit in the spectral domain when maser features at the same spatial position appeared in three or more adjacent spectral channels. The absolute positions of the maser features are tied to the positions of the phase calibrators 0629+104 (IC 443), 1748–253 (W 28), and 1801+010 (W 44). None of these are astrometric-quality calibrators, so while the *relative* positions of the brightest masers are limited by signal-to-noise to a few 10's of milliarcseconds, the *absolute* positions are probably no better than ± 100 mas.

The angular sizes of the maser features were also measured. For this data, where multiple non-overlapping fields were mapped from a single u,v data set, and several maser features are typically found in each field, it is very difficult to measure sizes of individual features by fitting to the u,v data. Instead, we fit two-dimensional Gaussians to individual maser features and the sizes were deconvolved from the synthesized beam using the AIPS task **JMFIT**. Tables 2, 3, and 4 show the results of these fits in the spatial and spectral domain for W 28, W 44, and IC 443, respectively.

3. Results

3.1. Distribution of Masers

In Figures 1, 2, and 3 we show images of the radio continuum for the SNR W 28, W 44, and IC 443, respectively. Rather than show the positions of individual features from Tables 2, 3 and 4 we show *regions* of OH(1720 MHz) concentrations overlaid on the grey-scales of the SNRs. Since the total size of the remnants is more than 30 arcminutes and we observed maser emission with $\sim 1.5''$ resolution, we must show these regions separately in order to distinguish individual maser

features. These are given in Figures 4-6.

For W 28 the apparent concentration of masers along the eastern and north-central part of the remnant is real. With our three pointings we should have been capable of detecting bright masers all across the face of W 28. The detections are presumably telling us about the extent of the interaction of the shock with the adjacent molecular cloud. Comparing these findings with Frail et al. (1994a) we detect 41 individual features versus their 26 detections. All of the bright masers detected by Frail et al. (1994a) are seen in our data but we fail to detect some of their weaker masers (< 100 mJy) presumably due to our higher noise level. In Figure 4a-4f we show the expanded regions of W 28, with the position of unresolved maser features marked by filled circles and resolved features by ellipses. The order of magnitude improvement in resolution between these and the earlier W 28 data shows that several of the original spots were in fact blended features. This is most dramatic in the region denoted as W 28-OH E (see Fig. 4e). Instead of the four masers detected at $15''$ resolution by Frail et al. (1994a) there are at least two dozen separate masers in this region at $1.5''$ resolution.

Similar numbers of masers (25) are found for W 44 but in IC 443 we discovered only six masers. A possible explanation for the relative paucity of masers in IC 443 will be discussed in §4.3. Like W 28, the masers in W 44 are concentrated in several regions, with the largest number of masers located near where the densest part of the molecular cloud is in physical contact with the remnant (Wootten 1977). The masers in all three remnants appear along the continuum edges of the synchrotron emission (see Figs. 4-6). This is most apparent in W 28-OH E and W 44-OH E, where the masers are plentiful enough to show that they lie along a line traced by the continuum contours. OH main-line masers have been found in linear arrangements before. W75N is a notable example with a N-S line of OH masers and a velocity spread of 9 km s^{-1} over its full $1.5''$ extent (Haschick et al. 1981, Baart et al. 1986). These observations have been interpreted alternatively as masers delineating a rotating protostellar disk (Haschick et al. 1981), or masers along the edge of an HII region, in gas compressed by an expanding shock (Baart et al. 1986). For the OH(1720 MHz) masers being discussed here, their close location near the edge of the non-thermal radio continuum emission is suggestive. The synchrotron emission results from particle acceleration in a shock, either in the outer blast wave or the reverse shock propagating into the ejecta (Blandford & Eichler 1987). Thus we favor an interpretation where the OH(1720 MHz) masers are located in the shock-compressed gas behind this region.

3.2. Maser Kinematics

The velocity of the masers in W 44 and IC 443 have a low dispersion ($< 1\text{-}2 \text{ km s}^{-1}$) about a mean value that agrees with the systemic velocity of the remnant (see §4.2 and 4.3). This point was noted earlier for the SNRs studied by Frail et al. (1996) and in fact they concluded that the velocity of the OH(1720 MHz) masers could be used to derive a kinematic distance to the remnants. The masers in W 28 appear to be an exception to this rule. There is a broad

distribution of maser velocities in Table 2, ranging from 4.8 km s^{-1} in W 28-OH A to 16 km s^{-1} in W 28-OH E. The velocity dispersion of the masers within individual regions is small, typically $1\text{-}2 \text{ km s}^{-1}$. On the larger scale there are large velocity difference across the remnant, reaching a maximum at W 28-OH E and falling away in regions both to the north and south.

We plot the velocity of these maser features as a function of angular distance from the remnant center in Figure 7. Velocities of maser features which lie closest to the center of W 28 are the smallest. There is a gradual increase from $V_{lsr}=5 \text{ km s}^{-1}$ at $\theta = 3'$ to $V_{lsr}=8 \text{ km s}^{-1}$ at $\theta = 14.5'$. At the edge of the remnant ($\theta = 14.5'$) the velocity dispersion increases sharply. This confluence of large positive velocities near the region where W 28 is in direct contact with the molecular cloud as mapped by Wootten (1981) was noted by Frail et al. (1994a). However, it is clear from Figure 7 that a simple geometric model such as a tilted disk or expanding sphere does not fit the velocity profile. We will return to this point in §4.1.

3.3. Angular Diameters of the Maser Spots

The brightness temperatures calculated for the OH(1720 MHz) emission features in Tables 2-4 range from about 2×10^4 to 10^8 K . This result, together with their narrow linewidths, leaves little doubt that the emission is amplified, stimulated emission (i.e. masers). Even the weakest emission sources have brightness temperatures much larger than expected in the molecular environment. We estimate that the continuum emission from the three SNRs, which are acting as background sources for the maser amplification process, is $10\text{-}80 \text{ K}$. Based on the brightness temperatures given above, this implies lower limits to the optical depths τ for the OH(1720 MHz) lines of -8 to -16 .

There is a range of apparent angular sizes for the maser features in Tables 2-4. Our deconvolution process has measured spot sizes on the order of $0.5''\text{-}0.9''$ for a number of features, and still other features are distinctly larger than the synthesized beam. Several maser spots are non-circular with aspect ratios larger than that of the synthesized beam. The orientation of the major axis of these non-circular features (Figs. 4-6) show no apparent pattern; they are neither aligned with each other nor do they trace the continuum contours. At the distance of these remnants the “resolved” maser spots ($\theta > 2''$) correspond to linear sizes of $\sim 10^{17} \text{ cm}$. Three possible origins exist for the spot sizes that we see: 1) they may be intrinsic maser spot sizes, 2) they may be broadened by multipath scattering in the ionized medium along the line of sight, or 3) they are due to multiple maser features within the synthesized beam. We favor the third explanation and we argue this point below.

The apparent maser spot sizes in Tables 2-4 are well in excess of the expected intrinsic sizes. Observations of the OH(1720 MHz) masers in the compact HII region W3(OH) give sizes less than 1.2 mas (Mashedier et al. 1994). The theory for the inversion of the OH(1720 MHz) line predicts $\tau \sim -20$ for the conditions we expect in these remnants (Elitzur 1976). Converting this to a angular size using the background continuum levels discussed above, we estimate intrinsic angular

sizes between 1 and 100 mas. Both of these estimates of intrinsic size are well below the angular diameters that we observe. Some angular broadening of the intrinsic maser sizes may be expected from interstellar scattering. In fact, Gwinn, Bartel & Cordes (1993) report an excess of scattering for the Vela and Crab pulsars, attributed to their respective SNRs and Spangler, Fey & Cordes (1987, and references therein) note several examples of enhanced scattering of sources along lines of sight that pass near SNRs. However, the amount of scattering that the angular diameters in Tables 2-4 imply is excessive, exceeding the magnitude seen towards such well-known lines of sight as the Galactic center (Frail et al. 1994b). Furthermore, there is no indication of excess scattering in the pulse profiles of PSR B0611+22 and PSR B1853+01 (Taylor, Manchester & Lyne 1993), the pulsars which are either behind or in IC 443 and W 44, respectively. The pulsar PSR 1758–23 toward W 28 is a special case and does show a broad scattering tail in its pulse profile. From the amount of temporal broadening in PSR 1758–23 and upper limits to the angular diameter of a nearby extragalactic source, Frail, Kulkarni & Vasisht (1993) constrain the SNR-scattering screen geometry and give a prediction for the angular diameter of point sources seen at W 28. At 1720 MHz the angular broadening in W 28 is expected to be between 150 and 500 mas. This is large but again well below the values we measure here. The simplest explanation consistent with the available data is that the elongated features that we see are a blend of unresolved maser features near the same velocity. Thus our computed brightness temperatures are *lower limits* to the true brightness temperatures. We have already seen how increasing the resolution by an order of magnitude in W 28 (15'' to 1.5'') resulted in the discovery of many more features. If we are correct, then a similar increase should be seen when higher resolution observations are made.

3.4. Zeeman Splitting and Magnetic Fields

Since we recorded all four parallel- and cross-polarization products from each antenna pair, we can calculate the full set of Stokes parameters (**I**, **Q**, **U**, **V**) for each line. Approximately half of our maser features show significant signal in the Stokes **V** profiles. The number of features detected in the **V** images is probably limited due to sensitivity effects, since the features with the weakest **I** signal are the ones in which we do not detect circularly polarized emission. When the polarized signal is located in the **V** images it is found to coincide on the sky to within one-tenth of a synthesized beam ($\sim 5 \times 10^{15}$ cm) to the emission on the corresponding **I** images. This positional coincidence is a strong argument that the **V** signal is due to the Zeeman effect. Many of the **V** profiles detected have the classical antisymmetric “S” shape about the line center. This also strongly supports the Zeeman splitting interpretation.

When the Zeeman splitting is small compared to the intrinsic (Doppler) linewidth, the Stokes **V** profile is proportional to the frequency derivative of the Stokes **I** profile (Heiles et al. 1993). Thus a fit of the **V** profile to the derivative of the **I** profile yields a measurement of the line-of-sight magnetic field, $V=C dI/d\nu$, where $C=0.6536 B_{\parallel}$ Hz μG^{-1} . The proportionality constant that we use is the same as Yusef-Zadeh et al. (1996) since our definitions of **I** and **V** are identical.

Figures 8 and 9 show sample results of the Stokes and derivative spectra for maser features in W 28 and W 44, respectively. In IC 443 we detect none of the typical “S” profiles in \mathbf{V} and thus a line-of-sight field cannot be estimated in the same manner. Table 5 lists the results of the Stokes \mathbf{V} fitting for the features in all three supernova remnants and when possible, the values of B_{\parallel} . In both W 28 and W 44 the strength of the field is within a factor of three of $B_{\parallel}=0.2$ mG at *all* locations. The direction of the field throughout each remnant is also constant, implying the existence of well-ordered magnetic fields over pc-sized distances.

Strictly speaking, the relation used above is valid only for thermal absorption and emission lines. The interpretation of polarization measurements from maser observations is dependent on the specific model adopted for polarized radiative transfer. Nedoluha & Watson (1992) conclude that the standard thermal relationship is an excellent approximation of B_{\parallel} for observations of water masers, if they are not strongly saturated, despite the complications of the maser radiative transfer.

Elitzur (1996, 1997) has derived a general polarization solution for arbitrary Zeeman splitting, which reproduces the limits of zero and very large splitting (compared to the linewidths) studied by Goldreich et al. (1973) as long as the masers are in the fully saturated regime. In particular, Elitzur’s solutions span the range where the Zeeman splitting is comparable to or slightly less than the linewidth. For OH, this condition occurs at field strengths of a few milliGauss. The solution in this regime has a similar functional form to that of thermal emission, but the dependence of the magnitude of Stokes V on the angle (θ) between the propagation direction and the magnetic field direction is somewhat different. According to Elitzur (1997), masers require smaller fields to produce the same amount of circular polarization as thermal emission. Thus our estimate of the magnetic fields given in Table 5 may be overestimates, by as much as factors of 2 to 4, depending on whether or not the 1720 MHz masers are saturated. These estimates of B_{\parallel} are five to ten times smaller than that found near the Galactic center by Yusef-Zadeh et al. (1996).

Table 5 also lists the peaks of Stokes parameters \mathbf{Q} and \mathbf{U} , the derived fractional linear polarization ($P_l = \frac{\sqrt{U^2+Q^2}}{I}$) and the polarization position angle $\chi = 0.5 \times \tan^{-1} \frac{U}{Q}$, where they were detected for all three remnants. According to Elitzur (1997), for the case of small splitting compared to the Doppler width, θ , the angle between the propagation direction and the magnetic field can be determined directly from a measurement of the linear polarization in the absence of Faraday rotation. Nedoluha and Watson (1990) suggest that the amount of linear polarization observed must depend on the saturation regime in which the masers are to be found, and indeed the linear polarization results of Goldreich et al. (1973), are also based on how saturated the masers are. From our current observations, we have no independent measure of the saturation of the masers, and so we have not used the linear polarization measurements to derive θ . The relatively small ($\leq 10\%$) linear polarization that we measure in these observations probably suggests that the masers are not operating in the completely saturated regime (Nedoluha & Watson 1990).

4. Discussion

4.1. W 28 (G 6.4–0.1)

Wootten (1981) has summarized the observational evidence that W 28 is interacting with a molecular cloud. The case rests on morphological and kinematic signatures. DeNoyer (1983) looked for, but did not find, evidence for a shock in the form of abundance enhancements of various species. On the eastern edge of W 28 there is a $5' \times 15'$ cloud that can be traced in absorption in the OH(1667 MHz) main-line (Pastchenko & Slysh 1974) and H₂CO at 4.8 GHz (Slysh et al. 1980), as well as in emission from ¹²CO(1-0) and ¹³CO(1-0) (Wootten 1981). This crescent-shaped cloud at $V_{lsr}=7$ km s⁻¹ bends around the SNR along its eastern edge and appears to make contact with W 28 at a prominent “kink” in the radio continuum emission (Velusamy 1987). The line widths of several molecular species (HCO⁺, CO, H₂CO) broaden significantly in the 7 km s⁻¹ cloud as one moves toward the SNR. This is nicely shown in Slysh et al. (1980) for the H₂CO absorption. In addition, the gas density, as traced by ¹³CO(1-0) and HCO⁺, peaks near this contact point (Wootten 1981). The average density in the cloud, determined from H₂CO, is 2.5×10^4 cm⁻³ (Wootten 1981), although regions of much higher density are implied by the detection of HCO⁺. The pre-shock kinetic temperature is likely $T_k \sim 15$ K (DeNoyer 1983).

Together, the morphology and kinematics of this 7 km s⁻¹ cloud has prompted several of the above authors to argue that its characteristics were being shaped by the impact of the shock from the W 28 SNR. However, the systemic velocity of W 28 appears to be much larger than this value. HI absorption measurements by Radhakrishnan et al. (1972) detect two discrete features at 7.3 km s⁻¹ and 17.6 km s⁻¹ against W 28. Similar lines are seen in H₂CO and OH (Pastchenko & Slysh 1974, Slysh et al. 1980). The velocity centroid determined from H α filaments in W 28 is 18 ± 5 km s⁻¹ (Lozinskaya 1974). If the systemic velocity of W 28 is close to 17.6 km s⁻¹, as the absorption and emission data suggests, then what is the relationship of the 7 km s⁻¹ molecular cloud to the SNR and what is the source of the broad distribution in the maser velocities as discussed in §3.2? We suggest that the entire 7 km s⁻¹ molecular cloud ($M=3.2 \times 10^3 M_\odot$) has been accelerated by the SNR shock along our line of sight, giving it a velocity of ~ -10 km s⁻¹ from the systemic velocity of W 28. The masers are collisionally excited by H₂ molecules in this cloud as well as other clouds with no blueshifted velocity component along the line-of-sight. This may be the origin of the broad range of maser velocities that we see in W 28, in contrast with all the other SNRs we have studied to date.

4.2. W 44 (G 34.7–0.4)

W 44 lies at the base of the Aquila supershell (GS 034–06+65), and is probably one of many SNRs driving its expansion (Maciejewski et al. 1996). The wealth of observations at all wavebands has recently been summarized by Giacani et al. (1997). Here we will review the evidence that the SNR is interacting with a molecular cloud. Wootten (1977) was the first to suggest that this

was the case on the basis on $^{12}\text{CO}(1-0)$ and $^{13}\text{CO}(1-0)$ observations. Near the eastern edge of the remnant the CO line widths, column density and temperature all increase. Moreover, he interpreted a velocity gradient seen in the CO lines as being due to a massive shell ($M=2.5\times 10^4 M_\odot$) expanding at 4 km s^{-1} toward the observer. In H_2CO absorption away from the remnant Slysh et al. (1980) observe gas at the systemic velocity of W 44 (45 km s^{-1}) but see a velocity discontinuity as they move inward along the eastern continuum edge ($\Delta V \simeq 5 \text{ km s}^{-1}$). This was also interpreted as a cloud accelerated by W 44. A high-velocity HI shell centered on W 44 was found by Koo & Heiles (1995). While they argue that this shell has been accelerated by W 44 it lies interior to the outer edge of the SNR as defined by the continuum emission. Koo & Heiles develop a model in which the HI shell was produced by mass outflow from the progenitor star *prior* to the supernova event, and thus is not part of the current interaction with the ambient molecular gas.

As in the case of W 28, DeNoyer (1983) could not find any evidence for shock enhancement of molecular species (e.g. CS, HCN, HCO^+) toward W 44. She further questions the interpretation of the broad line widths and velocity gradients seen by Wootten (1977) and Slysh et al. (1980) and suggests that rather than being evidence for acceleration, they are due to separate but overlapping velocity components. Perhaps the strongest independent evidence for an interaction of W 44 with a molecular cloud comes from recent ISO observations of [OI], an important coolant in shocked molecular gas (Reach & Rho 1996). It was found that the [OI] was brightest along the eastern edge of the remnants, and in fact peaked at the location of the OH(1720 MHz) masers. A J-shock model predicting the intensity of the [OI] line constrains the product of the density and shock velocity to be $10^5 \text{ cm}^{-3} \text{ km s}^{-1}$.

In §3.4 we showed that the line-of-sight magnetic field B_\parallel in both W 44 and W 28 was of the order of 0.2 mG. Recall that this may be an upper limit in B_\parallel because we have used the thermal constant to relate the splitting that is observed in the Stokes \mathbf{V} profiles to the magnitude of the field. By the same token the expectation value of the *total* magnetic field $B=2\times B_\parallel$. Recognizing this uncertainty in the discussion that follows we adopt $B=0.2 \text{ mG}$, a value which is consistent with typical magnetic fields in molecular clouds of density $n_{\text{H}_2} = 10^4 \text{ cm}^{-3}$ (Myers & Goodman 1988). The Alfvén velocity V_A in this gas is 4 km s^{-1} .

A magnetic field of 0.2 mG has a corresponding magnetic field pressure $p_B=B^2/8\pi$ of $2\times 10^{-9} \text{ dyne cm}^{-2}$. This can be compared to the thermal gas pressure $p_g = 2 n_e kT$ driving the expansion, as estimated from the hot X-ray emitting gas filling the interior of the remnants. In W 44 Jones, Smith and Angellini (1993) derive $p_g = 6 - 8 \times 10^{-10} \text{ dyne cm}^{-2}$, while for W 28 $p_g \sim 6 \times 10^{-10} \text{ dyne cm}^{-2}$ (Rho et al. 1996). Both of these values are much larger than the ambient ISM pressure of $p_o = 5 \times 10^{-13} \text{ dyne cm}^{-2}$ (Kulkarni & Heiles 1988). We conclude on the basis of these estimates that $p_B \geq p_g \gg p_o$ and thus the magnetic field exerts considerable influence on both the dynamics and the structure of the shock.

The presence of a magnetic field in the molecular gas limits the postshock compression to $\sqrt{2}V_s/V_A$, where V_s is the shock velocity (Draine & McKee 1993). Lozinskaya (1974) has

measured a mean V_s for the H α filaments in W 28 of 45 km s $^{-1}$, while optical line ratios (Bohigas et al. 1983, Long et al. 1991) yield values that are typically twice this. In the younger remnant W 44 Koo & Heiles (1995) derive $V_s=330$ km s $^{-1}$ from modeling HI data, while Rho et al. (1994) derive $V_s=630$ km s $^{-1}$ from X-ray observations. Since these estimates are based on measurements made in neutral and ionized gas with densities between 1 and 100 cm $^{-3}$, we must scale them by the square root of the density ratio to obtain a value for V_s where the OH(1720 MHz) maser emission is seen. The resulting values (assuming $n_{\text{H}_2} \sim 10^4$ cm $^{-3}$) are highly uncertain but do not exceed $V_s=10$ km s $^{-1}$. Thus the maximum compression of the gas and magnetic field in the post-shock molecular cloud is of order two to three times the ambient value. A related issue is the question of the nature of the shock. Given the low value of V_s derived above and the relative strength of the magnetic pressure compared to the thermal gas pressure (i.e. $p_B \geq p_g$), we think it unlikely that the shock will dissociate the H $_2$ molecules. Whether pre- and post-shock conditions change gradually (C-type) or suddenly (J-type) cannot be answered without knowledge of the degree of ionization in the molecular cloud ahead of the shock (Draine & McKee 1993). This issue has considerable bearing on the type of chemistry that occurs behind the shock and as a result the relative abundances of various molecules, including OH.

4.3. IC 443 (G 189.1+3.0)

Since DeNoyer (1979) first found shocked OH in absorption against IC 443, it has become the best laboratory we have for the study of the interaction between a supernova remnant shock and a molecular cloud. At $(l, b) = (189.1, +3.0)$ the physical conditions of both the pre-shock and post-shock gas for IC 443 can be determined without the usual confusion from unrelated galactic emission. The neutral hydrogen (HI) and dust were studied by Braun & Strom (1986), revealing swept-out cavities, shock heated dust and accelerated HI gas. Shocked molecular gas along the S-shaped ridge demarcating the interaction, was observed in the vibrational lines of H $_2$ by Burton et al. (1988). Numerous studies have been made of molecules at millimeter and submillimeter wavelengths (e.g. Huang, Dickman & Snell 1986, White et al. 1987, Wang & Scoville 1992, van Dishoeck, Jansen & Phillips 1993). Some evidence exists for shock chemistry processing (i.e. depletions or enhancements for the abundances of various molecular species relative to their interstellar values) but not always in accordance with existing shock models. Part of the difficulty may be that IC 443 cannot be modeled by a single shock but rather requires a mixture of both J-type and C-type shocks (Burton et al. 1990, Wang & Scoville 1992).

With such overwhelming evidence for an interaction, it may at first seem puzzling why we have detected so few masers toward IC 443. The 6 masers in Table 3 are all found within clump “G”, one of a series of broad-line molecular clumps first imaged in the CO line by DeNoyer (1979) and continued by Huang et al. (1986). Clump G or IC 443G is located near the center of the optical remnant but forms the western-most edge of a ring of shocked molecular gas that can be traced in the lines of CO, HCO $^+$ and H $_2$. The systematic variation of the peak velocity

with position prompted Dickman et al. (1992) and van Dishoeck et al. (1993) to model the shocked gas as a tilted molecular ring, with the shock in IC 443G transverse to the line of sight. Additional evidence for this shock geometry comes from ^{12}CO emission lines and main line OH absorption lines, both of which show evidence for pre-shock and post-shock gas (e.g. DeNoyer & Frerking 1981). In IC 443B where the shock is thought to be mostly along the line of sight to the observer, there is a clear separation in velocity between the shocked and accelerated gas (the broad asymmetric profiles) and the unshocked ambient gas (narrow profiles) (van Dishoeck et al. 1993). In IC 443G the broad line ($\Delta V \simeq 30 \text{ km s}^{-1}$) remains but there is a narrow self-absorption feature superimposed on emission lines like ^{12}CO and HCO^+ at a velocity between -4 and -5 km s^{-1} (White et al. 1987, van Dishoeck et al. 1993, Tauber et al. 1994). Such line profiles are expected from projection effects for a transverse shock (see Turner et al. (1992) for a contrary picture). The self-absorption is then due to cooler foreground gas, presumably the unshocked ambient gas whose velocity is the systemic velocity of the remnant (White et al. 1987).

The presence of a transverse shock in IC 443G may have important implications for the lack of masers seen elsewhere in IC 443. In the OH(1720 MHz) survey paper by Frail et al. (1996) it was noted that in all instances the OH masers were detected at or near the systemic velocity of the supernova remnant. This was the case even when it was clear that the masers distributed around a remnant arose from regions where the shock was propagating into gas with very different properties (e.g. CTB 37A). We note that the velocities of our masers in IC 443G are also clustered close to the velocity of the the ambient gas ($\sim -5 \text{ km s}^{-1}$). In Frail et al. (1996) we suggested that this was due to the fact that, similar to the case of stellar H_2O masers, the path of maximum amplification occurs when the acceleration produced by the shock is transverse to the line of sight. It is along this direction that the velocity gradient is minimized and the largest coherent pathlengths needed for bright maser emission are maintained. In IC 443G we have for the first time clear evidence for the existence of a transverse shock and thus compelling proof that tangential amplification is important in the excitation of the OH(1720 MHz) masers. The lack of masers elsewhere in IC 443, where the shock geometry is less favorable indirectly supports this hypothesis. An alternate explanation for why the OH(1720 MHz) maser velocities are close to the systemic velocity of the remnant is that they are excited ahead of the shock in the unshocked ambient gas. X-rays propagating from the shock into the dense molecular material can form an X-ray dissociation region (XDR, Maloney, Hollenbach & Tielens 1996) with the densities and temperatures needed to invert the 1720 MHz line of OH. However, Burton et al. (1990) showed that the luminosity of the infrared lines in IC 443 such as [OI] are too large to be explained by X-ray heating and that a shock model was preferred.

IC 443G has been studied in a number of millimeter and submillimeter lines by several groups (White et al. 1987, Ziurys et al. 1989, Turner & Lubowich 1991, Turner et al. 1992, van Dishoeck et al. 1993, Tauber et al. 1994), allowing for accurate physical parameters to be determined. At the highest angular resolution provided by interferometric observations ($\sim 5''$) IC 443G breaks into two sub-clumps called GI and GII by van Dishoeck et al. (1993) (G1 and G2 by Tauber et al. 1994). Five of the six masers in Table 3 lie near the peak of GI, while our weakest maser is

closer to GII. The self-absorption of CO and other molecules in GII was used by van Dishoeck et al. (1993) to constrain the gas kinetic temperature and density of the ambient (unshocked) gas of $T_k=10\text{-}20$ K and $n_{\text{H}_2} \sim 10^4 \text{ cm}^{-3}$. The parameters for the postshock gas are more controversial and a range of densities and temperatures seem to be present. Ziurys et al. (1989) used NH_3 to derive $T_k=33$ K and argued that $n_{\text{H}_2} > 10^5 \text{ cm}^{-3}$ because they detected HCO^+ . A detection of H_2CO by Turner & Lubowich (1991) suggests much higher temperatures ($T_k > 300$ K) and densities ($n_{\text{H}_2} \simeq 10^7 \text{ cm}^{-3}$). The multitransitional studies by Turner et al. (1992) and van Dishoeck et al. (1993) required at least two components to fit the observations of molecules in IC 443G. The parameters of van Dishoeck et al. (1993) fits give $n_{\text{H}_2} \simeq 10^5 \text{ cm}^{-3}$, $T_k \sim 80$ K for the low density component and $n_{\text{H}_2} \simeq 3 \times 10^6 \text{ cm}^{-3}$, $T_k \sim 200$ K for the high density component. Turner et al. (1992) give similar values.

Based on these density and temperature measurements it is possible to relate our observations to the Elitzur (1976) model which explains the inversion of the OH(1720 MHz) maser line. With $T_k=10\text{-}20$ K it is unlikely that the OH is excited in the ambient gas, since the pump efficiency is much reduced below 25 K and fails to function below 15 K. It is equally improbable that the inversion is occurring in the high density component of IC 443G. At $T_k > 200$ K the excitation of the 1612 MHz satellite line begins to dominate over 1720 MHz and at $n_{\text{H}_2} \gg 10^5 \text{ cm}^{-3}$ collisional de-excitation depopulates the inversion (see also Pavlakis & Kylafis 1996a). This leaves the low density component ($n_{\text{H}_2} \simeq 10^5 \text{ cm}^{-3}$, $T_k \sim 80$ K), which according to Elitzur (1976) has the necessary density and temperature capable of exciting the 1720 MHz masers. With more accurate modeling it should be possible to predict the strength of the inversion and the size of the masing regions in IC 443G, as was done approximately for W 28 (Frail et al. 1994).

4.4. OH(1720 MHz) As A Tracer of Cosmic Ray Acceleration Sites

Supernova remnant shocks have long been proposed as the acceleration sites for cosmic rays (see reviews by Blandford & Eichler 1987, Biermann 1997) but direct observational proof is still lacking. Arguments based on energetics and spectra demonstrate in a self-consistent way that SNRs can provide the bulk of cosmic rays seen above the “knee” near 5×10^{15} eV. For example, Duric et al. (1995) have shown the cosmic rays in M33 can be maintained by the observed SNR population. Moreover, the non-thermal spectrum of the SNRs in our Galaxy (produced by synchrotron emission from relativistic electrons) agree with the observed cosmic ray spectrum after accounting for propagation effects. Powerful support of this argument comes from the recent detection of X-ray synchrotron emission from SN 1006 (Koyama et al. 1995), as it demonstrates that SNRs can accelerate electrons with the correct spectrum to energies ≥ 200 Tev (Reynolds 1996 but see Mastichiadis & de Jager 1996 for a different viewpoint).

While it may never be possible to detect cosmic rays from SNRs directly, collisions between cosmic rays and the atomic or molecular gas in the ISM produce π^0 muons, which in turn decay to gamma rays. Indeed, the distribution of the diffuse component of high energy gamma rays

(>100 MeV) follows the galactic distribution of gas tracers like CO and HI nicely (Bloemen 1989). Embedded in the diffuse emission are discrete gamma ray sources for which identification has been more problematic. Early identifications with the COS-B satellite included young pulsars such as Vela and the Crab and the quasar 3C 273 (Swanenberg et al. 1981). The EGRET instrument on the Compton Gamma Ray Observatory has continued to find more young pulsars (Nel et al. 1996) and several active galactic nuclei, but a stubborn number of the unresolved EGRET sources remain unidentified. The second EGRET catalog and its supplement have increased the original 22 COS-B sources with $|b| \leq 10^\circ$ to a total of 46 (Thompson et al. 1995, 1996).

The majority of these unidentified gamma ray sources are likely nearby neutron stars, but a small subset could originate when cosmic rays, accelerated in a supernova remnant shock, encounter the dense molecular gas into which the remnant is expanding into and compressing. This suggestion was first made for several of the COS-B sources by Montmerle (1979), Morfill, Forman & Bignami (1984) and Pollock (1985). More recently both Sturmer & Dermer (1995) and Esposito et al. (1996) have found examples of unidentified EGRET sources which are at the same position as galactic SNRs with a low probability of chance coincidence. In particular, Esposito et al. (1996) have looked at a sample of 14 radio-bright SNRs and found 5 candidates: W 28, W 44, IC 443, Monoceros and γ Cyg. The EGRET sources in Monoceros and γ Cyg are both found interior to the remnant and are likely young neutron stars. Brazier et al. (1996) have recently detected an X-ray source within the EGRET error circle of γ Cyg with characteristics similar to Geminga. They argue that the gamma ray emission is from a young, radio-quiet pulsar.

The three remaining SNRs also have known pulsars in their vicinity (PSRs B0611+22, B1853+01 and B1758–23), two of which are within an EGRET error circle. We cannot completely discount that the gamma ray emission toward these SNRs originates from the pulsars (or a wind nebula); however, searches have been made for pulsed high energy emission without success (Nel et al. 1996). Furthermore, it is noteworthy that the three remaining SNR/EGRET coincidences are also our three best examples of a SNR/molecular cloud interaction, as traced by the detection of the OH(1720 MHz) maser transition. Figure 10 shows the positions of the 1720 MHz masers and the EGRET error circles overlaid on the radio continuum. Although the errors in position are relatively large, the EGRET sources are located near the edges of W 28, W 44, IC 443, not inside them. Moreover, for W 28 and W 44 the EGRET sources coincide with the quadrants where most of the masers are located. For W 28 this is the northeastern edge and for W 44 it is the eastern edge of the SNR. In the case of IC 443 the maser emission is less prominent (see §4.3 for an explanation) but the EGRET source is found on the eastern edge of the SNR where abundant neutral and molecular tracers indicate that a strong shock along our line of sight is encountering a molecular cloud (Braun & Strom 1986, Burton et al. 1988, van Dishoeck, Jansen & Phillips 1993).

The correlation of the EGRET sources with SNRs, in and of itself, is not a compelling proof that gamma rays originate as decay products from the collision of cosmic rays with the gas surrounding an SNR. However, the detection of the OH(1720 MHz) masers demonstrates the existence of gas at a density between 10^4 - 10^5 cm^{-3} which is in close proximity to the sites where

the cosmic rays are proposed to be accelerated. These density enhancements are expected to produce local hot spots of gamma ray emission above the background Drury, Aharonian & Völk 1994). The detection of the OH(1720 MHz) maser transition is much stronger evidence that a SNR is interacting with a molecular cloud than the detection of HI or CO clouds towards the SNR (e.g. Huang & Thaddeus 1986). Without a clear shock signature such detections have a high probability of being line of sight coincidences. On the other hand, since the OH(1720 MHz) line is thought to be collisionally excited by H₂ molecules heated by a shock (Elitzur 1976), it is an unambiguous tracer of such interactions.

The OH(1720 MHz) line not only supports the cosmic ray model for the origin of these EGRET sources as advocated by Sturmer & Dermer (1995) and Esposito et al. (1996), it provides a useful target list for future observations with more sensitive GeV satellites or instruments at TeV energies where the background is much reduced (Kifune 1995). There are a total of 17 SNRs towards which OH(1720 MHz) masers have been detected (Green et al. 1997 and references therein). The flux density of the gamma rays produced via π^0 decay depends directly on the fraction of the supernova blast energy E_0 that goes into accelerating the cosmic rays and the density of the gas, and inversely on the square of the distance to the SNR (Aharonian, Drury & Völk 1994, Drury et al. 1994). W 28, W 44, IC 443 are the closest SNRs. The remaining 14 SNRs all are more distant than 5 kpc and thus we would not expect these SNR detected as discrete EGRET sources given its sensitivity (Drury et al. 1994). However, they are important candidates for future searches and their detection at GeV or TeV energies would be a convincing proof of cosmic ray acceleration theories.

5. Conclusions

The observations presented here leave little doubt that the OH(1720 MHz) features that we have detected toward supernova remnants are masers. Estimates of the temperature and densities based on thermal molecular data agree with those used in the shock excitation model of Elitzur (1976). The limits on the maser optical depth and brightness temperatures are of the correct magnitude. The distribution of the masers behind the leading edge of the shock, as traced by the relativistic electrons, suggest that the lines originate in postshock gas. Clear evidence for this also exists in the specific case of IC 443, where the masers are positionally coincident with shocked gas (i.e. IC 443G). We have also shown that the maser velocities cluster around the systemic velocity of the remnant and the parent molecular cloud into which the shock is propagating. This, together with the existence of a transverse shock for IC 443, has been used to argue that the tangential amplification is important for the excitation of OH(1720 MHz) masers.

Despite this progress some uncertainty remains. The peculiar kinematics of W 28 do not fit this simple picture. The smooth gradient in velocity as one moves outward to the edge of the W 28 SNR, and the large increase in the velocity dispersion at the edge, are difficult to understand. A molecular cloud accelerated by the SNR toward the line-of-sight was offered as an explanation

but it is not a unique explanation nor is it an entirely satisfactory one. A first-ever measurement of the strength of the magnetic field in post-shock gas behind a supernova remnant has allowed us to demonstrate the dominance of magnetic pressure in these shocks. However, the details of the shock physics are still not clear. Is the shock dissociative or do the H_2 and OH survive the passage of the shock? Likewise the physical parameters of the pre- and post-shock gas are not well constrained except perhaps for IC 443. Better theoretical modeling of the shock and maser excitation process are needed. While it may be possible to infer the density and temperature of the gas from the masers lines alone, observations of millimeter and sub-millimeter lines should be used as an important check on the OH(1720 MHz) maser models. Higher angular observations with full Stokes parameters should also be pursued to measure the true intrinsic size of the OH(1720 MHz) masers (and hence T_b and τ) and to check that the derivation of magnetic fields from the Stokes \mathbf{V} profile fitting is not confused by unrelated, but overlapping features in the arcsecond beam.

This research has made use of NASA's Astrophysics Data System Abstract Service (ADS) and the Simbad database, operated at CDS, Strasbourg, France.

REFERENCES

- Aharonian, F. A., Drury, L. O'C., & Völk, H. J. 1994, *A&A*, 285, 645
- Baart, E. E., Cohen, R. J., Davies, R. D., Norris, R. P., & Rowland, P. R. 1986, *MNRAS*, 219, 145
- Ball, J. A., & Staelin, D. H. 1968, *ApJ*, 153, L41
- Biermann, P. L. in *Cosmic Winds and the Heliosphere*, eds. J. R. Jokipii, C. P. Sonett and M. S. Giampapa, in press, 1997
- Blandford, R. & Eichler, D. 1987, *Physics Reports*, 154, 1
- Bloemen, H. 1989, *ARA&A*, 27, 469
- Bohigas, J., Ruiz, M. T., Carrasco, L., Salas, L., & Herrera, M. A. 1983, *Rev Mex. Astron. Astrophys.*, 8, 155
- Braun, R., & Strom, R. G. 1986, *A&A*, 164, 193
- Brazier, K. T. S., Kanbach, G., Carramiñana, A., Guichard, J., & Merck, M. 1996, *MNRAS*, 281, 1033
- Burton, M. G., Hollenbach, D. J., & Haas, M. R., & Erickson, E. F. 1990, *ApJ*, 355, 197
- Burton, M. G., Brand, P. W. J. L., Geballe, T. R., & Webster, A. S. 1988, *MNRAS*, 231, 617
- Cesaroni, R., & Walmsley, C. M. 1991, *A&A*, 241, 537
- DeNoyer, L. K. 1979, *ApJ*, 232, L165
- DeNoyer, L. K. 1983, *ApJ*, 264, 141
- DeNoyer, L. K., & Frerking, M. A. 1981, *ApJ*, 246, L37

- Dickman, R. L., Snell, R. L., Ziurys, L. M., & Huang, Y. -L. 1992, *ApJ*, 400, 203
- Draine, B. T., & McKee, C. F. 1993, *ARA&A*, 31, 373
- Drury, L. O’C., Aharonian, & Völk, H. J. 1994, *A&A*, 287, 959
- Duric, N., Gordon, S. M., Goss, W. M., Viallefond, F., & Lacey, C. 1995, *ApJ*, 445, 173
- Elitzur, M. 1976, *ApJ*, 203, 124
- Elitzur, M. 1996, *ApJ*, 457, 415
- Elitzur, M. 1997, *ApJ*, submitted
- Esposito, J. A., Hunter, S. D., Kanbach, G., & Sreekumar, P. 1996, *ApJ*, 461, 820
- Frail, D. A., Kulkarni, S. R., & Vasisht, G. 1993, *Nature*, 365, 136
- Frail, D. A., Goss, W. M., & Slysh, V. I. 1994a, *ApJ*, 424, L111
- Frail, D. A., Diamond, P. J., Cordes, J. M., & van Langevelde, H. J. 1994b, *ApJ*, 427, L43
- Frail, D. A., Goss, W. M., Reynoso, E. M., Giacani, E. B., & Green, A. J. 1996, *AJ*, 111, 1651
- Giacani, E. B., et al. 1997, in preparation.
- Goldreich, P., Keeley, D. A., & Kwan, J. Y. 1973, *ApJ*, 179, 111
- Goss, W. M. 1968, *ApJS*, 15, 131
- Goss, W. M., & Robinson, B. J. 1968 *Astrophys. Lett.*, 2, 81
- Gray, M. D., Doel, R. C., & Field, D. 1991, *MNRAS*, 252, 30
- Green, A. J., Frail, D. A., Goss, W. M., & Otrupcek, R. 1997, (in preparation)
- Gwinn, C. R., Bartel, N., & Cordes, J. M. 1993, *ApJ*, 410, 673
- Hardebeck, E. G. 1971, *ApJ*, 170, 281
- Haschick, A. D., Reid, M. J., Burke, B. F., Moran, J. M., & Miller, G. 1981, *ApJ*, 244, 76
- Haynes, R., & Caswell, J. 1977, *MNRAS*, 178, 219
- Heiles, C., Goodman, A. A., McKee, C. F., & Zweibel, E. G. 1993 in “Protostars and Planets”, eds E. H. Levy and J. I. Lunine (University of Arizona Press: Tucson), p. 279
- Huang, Y. -L., & Thaddeus, P. 1986, *ApJ*, 309, 804
- Huang, Y. -L., Dickman, R. L., & Snell, R. L. 1986, *ApJ*, 302, L63
- Jones, L. R., Smith, A., & Angellini, L. 1993, *MNRAS*, 265, 631
- Kifune, T. 1995, *Aust. J. Phys.*, 48, 305
- Koo, B. -C., & Heiles, C. 1995, *ApJ*, 442, 679
- Koyama, K., Petre, R., Gotthelf, E. V., Hwang, U., Matsuura, M., Ozaki, M., & Holt, S. S. 1995, *Nature*, 378, 255

- Kulkarni, S. R. & Heiles, C. in *Galactic and Extragalactic Radio Astronomy*, 1988, eds G. L. Verschuur and K. I. Kellermann (New York: Springer Verlag), 95
- Long, K. S., Blair, W. P., Matsui, Y., & White, R. L. 1991, *ApJ*, 373, 567
- Lozinskaya, T. 1974, *Soviet Astr. Lett.*, 17, 603
- Maloney, P. R., Hollenbach, D. J., & Tielens, A. G. G. M. 1996, *ApJ*, 466, 561
- Maciejewski, W., Murphy, E. M., Lockman, F. J., & Savage, B. D. 1996, *ApJ*, 469, 238
- Mashedier, M. R. W., Field, D., Gray, M. D., Migenes, V., Cohen, R. J., & Booth, R. S. 1994, *A&A*, 281 871
- Mastichiadis, A., & de Jager, O. C. 1996, *A&A*, 311, L5
- Montmerle, T. 1979, *ApJ*, 231, 95
- Morfill, G. E., Forman, M., & Bignami, G. 1984, *ApJ*, 284, 856
- Myers, P. C., & Goodman, A. A. 1988, *ApJ*, 326, L27
- Nedoluha, G. E. & Watson, W. D. 1992, *ApJ*, 384, 185
- Nedoluha, G. E. & Watson, W. D. 1990, *ApJ*, 354, 660
- Nel, H. I. et al. 1996, *ApJ*, 465, 898
- Offer, A. R., van Hemert, M. C., & van Dishoeck, E. F. 1994, *J. Chem. Phys.*, 100, 362
- Pastchenko, M. I., & Slysh, V. I. 1974, *A&A*, 35, 153
- Pavlakis, K. G., & Kylafis, N. D. 1996a, *ApJ*, 467, 300
- Pavlakis, K. G., & Kylafis, N. D. 1996b, *ApJ*, 467, 309
- Pollock, A. M. T. 1985, *A&A*, 150, 339
- Radhakrishnan, V., Goss, W. M., Murray, J. D., & Brooks, J. W. 1972, *ApJS*, 24, 49
- Reach, W. T., & Rho, J. -H. 1996, *A&A*, 315, L277
- Rho, J. -H., Petre, R., Schlegel, E. M., Hester, J. J. 1994, *ApJ*, 430, 757
- Reynolds, S. P. 1996, *ApJ*, 459, L13
- Rho, J. -H., Petre, R., Pisarski, R., Jones, L. R. 1996, in “Röntgenstrahlung from the Universe” eds. H. U. Zimmermann, J. E. Trümper, and H. Yorke, MPE Report 263, p. 273
- Roberts, D. A., Crutcher, R. M., Troland, T. H., & Goss, W. M. 1993, *ApJ*, 412, 675
- Robinson, B., Goss, M. G., Yusef-Zadeh, F., Roberts, D. A., Frail, D. A. 1997, in preparation
- Spangler, S. R., Fey, A. L., & Cordes, J. M. 1987, *ApJ*, 322, 909
- Slysh, V. I., Wilson, T. L., Pauls, T., & Henkel, C. 1980, in “Interstellar Molecules”, IAU Symp. 87, ed. B. H. Andrew (D. Reidel: Dordrecht), p. 473
- Sturmer, S. J., & Dermer, C. D. 1995, *A&A*, 293, L17

- Swanenburg, B. N. et al. 1981, ApJ, 243, L69
- Tauber, J. A., Snell, R. L., Dickman, R. L., & Ziurys, L. M. 1994, ApJ, 421, 570
- Taylor, J. H., Manchester, R. N., & Lyne, A. G. 1993, ApJS, 88, 529
- Thompson, D. J. et al. 1996, ApJS, 107, 227
- Thompson, D. J. et al. 1995, ApJS, 101, 259
- Turner, B. E., & Lubowich, D. A. 1991, ApJ, 381, 173
- Turner, B. E., Chan, K. -W., Green, S., & Lubowich, D. A. 1992, ApJ, 399, 114
- Turner, B. E. 1969, ApJ, 157, 103
- Turner, B. E. 1982, Regions of Recent Star Formation, eds. R.S. Roger and P. E. Dewdney, Dordrecht: D. Reidel, 425
- van Dishoeck, E. F., Jansen, D. J., & Phillips, T. G. 1993, A&A, 279, 541
- Velusamy, T. 1987 in “Supernova Remnants and the Interstellar Medium”, IAU Collq. 101, eds. R. S. Roger and T. L. Landecker (Cambridge University Press: Cambridge), p. 265
- Wang, Z., & Scoville, N. Z. 1992, ApJ, 386, 158
- White, G. J., Rainey, R., Hayashi, S. S., & Kaifu, N. 1987, A&A, 173, 337
- Wootten, A. 1977, ApJ, 216, 440
- Wootten, A. 1981, ApJ, 245, 105
- Yusef-Zadeh, F., Uchida, K. I., & Roberts, D. 1995, Science, 270, 1801
- Yusef-Zadeh, F., Roberts, D. A., Goss, W. M., Frail, D. A., & Green, A. J. 1996, ApJ, 466, L25
- Ziurys, L. M., Snell, R. L., Dickman, R. L. 1989, ApJ, 341, 857

Fig. 1.— A 327 MHz radio continuum image (Frail, Kulkarni & Vasisht 1993) of the W 28 SNR with the location of the various regions of OH(1720 MHz) emission concentrations indicated. The beam size is 55" by 41" at position angle 69°, and the grey scale at the top is in mJy beam⁻¹. These regions are shown in more detail in Fig. 4.

Fig. 2.— A 1442 MHz radio continuum image (Giacani et al. 1997) of the W 44 SNR with the location of the various regions of OH(1720 MHz) emission concentrations indicated. The beam size is 15" , and the grey scale at the top is in mJy beam⁻¹. These regions are shown in more detail in Fig. 5.

Fig. 3.— A 330 MHz radio continuum image (Kassim, private communication) of the IC 443 SNR with the location of the OH(1720 MHz) emission as indicated. The beam size is 80" by 70" at position angle 50°, and the grey scale at the top is in mJy beam⁻¹. This region is shown in more detail in Fig. 6.

Fig. 4.— Individual regions of OH(1720 MHz) emission concentrations (a-f) in the W 28 SNR. For each region the radio continuum contours are plotted and labeled in mJy beam⁻¹. Individual OH(1720 MHz) masers are also plotted with exaggerated sizes to reflect the apparent OH(1720 MHz) spot sizes as determined by our fitting process (see §2). The size of the ellipse is ten times the angular diameters given in Table 2. Unresolved features are indicated by a filled circle.

Fig. 5.— Identical to Fig. 4. except for the W 44 SNR.

Fig. 6.— Identical to Fig. 4. except for the IC 443 SNR.

Fig. 7.— The distribution of maser velocities (LSR) across W 28. The geometric center of W 28 is taken to be at $\alpha = 17^h 57^m 47^s$, $\delta = -23^\circ 20' 24''$ (B1950). Individual maser features are plotted with open circles, the diameter of which is proportional to the logarithm of their peak flux density.

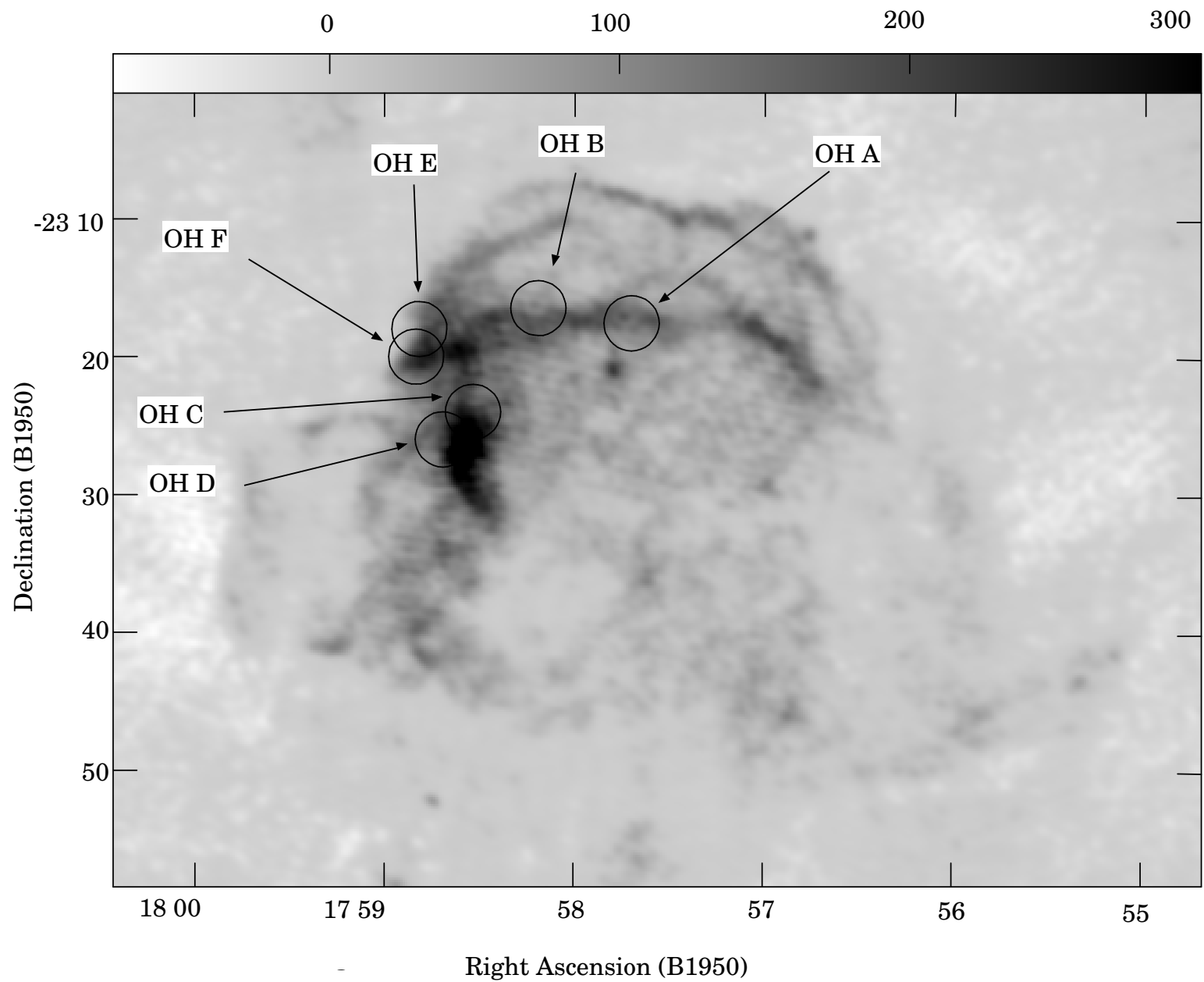
Fig. 8.— Stokes parameter spectra for maser feature 3 (see Table 2) in the W 28 SNR. Shown with the **V** spectrum, as a dashed line, is the frequency derivative of the **I** spectrum, scaled by the magnetic field strength.

Fig. 9.— Identical to Fig. 8, except for maser feature 11 (see Table 3) in the W 44 SNR.

Fig. 10.— The location of discrete gamma-ray sources with respect to W 28, W 44 and IC 443 as detected by the EGRET experiment on the Compton Gamma Ray Observatory. Large ellipses are the EGRET error circles, smaller circles are the regions of OH(1720 MHz) emission.

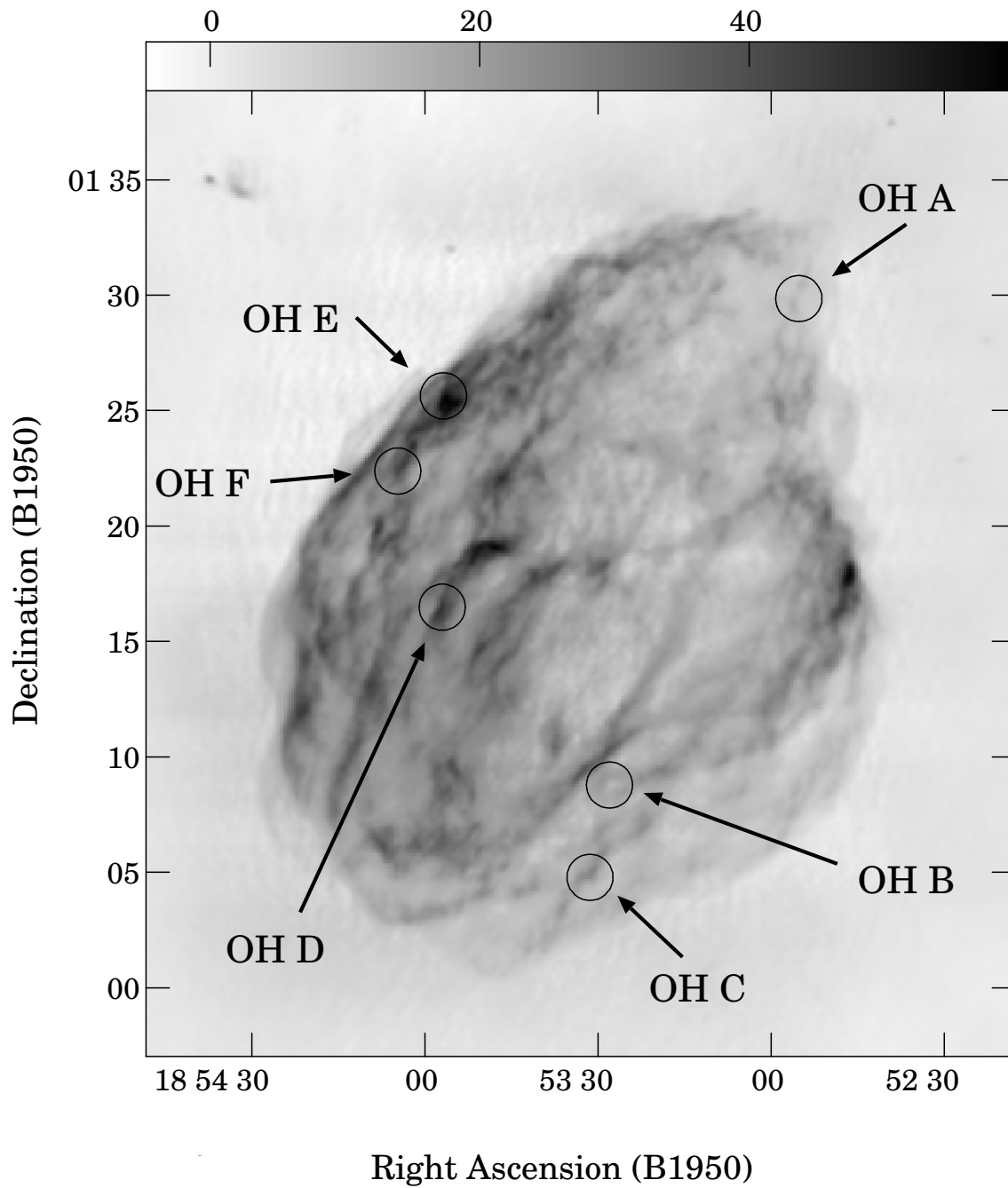
W28 SNR with OH Masers

327 MHz Continuum Grey Scale in mJy/beam



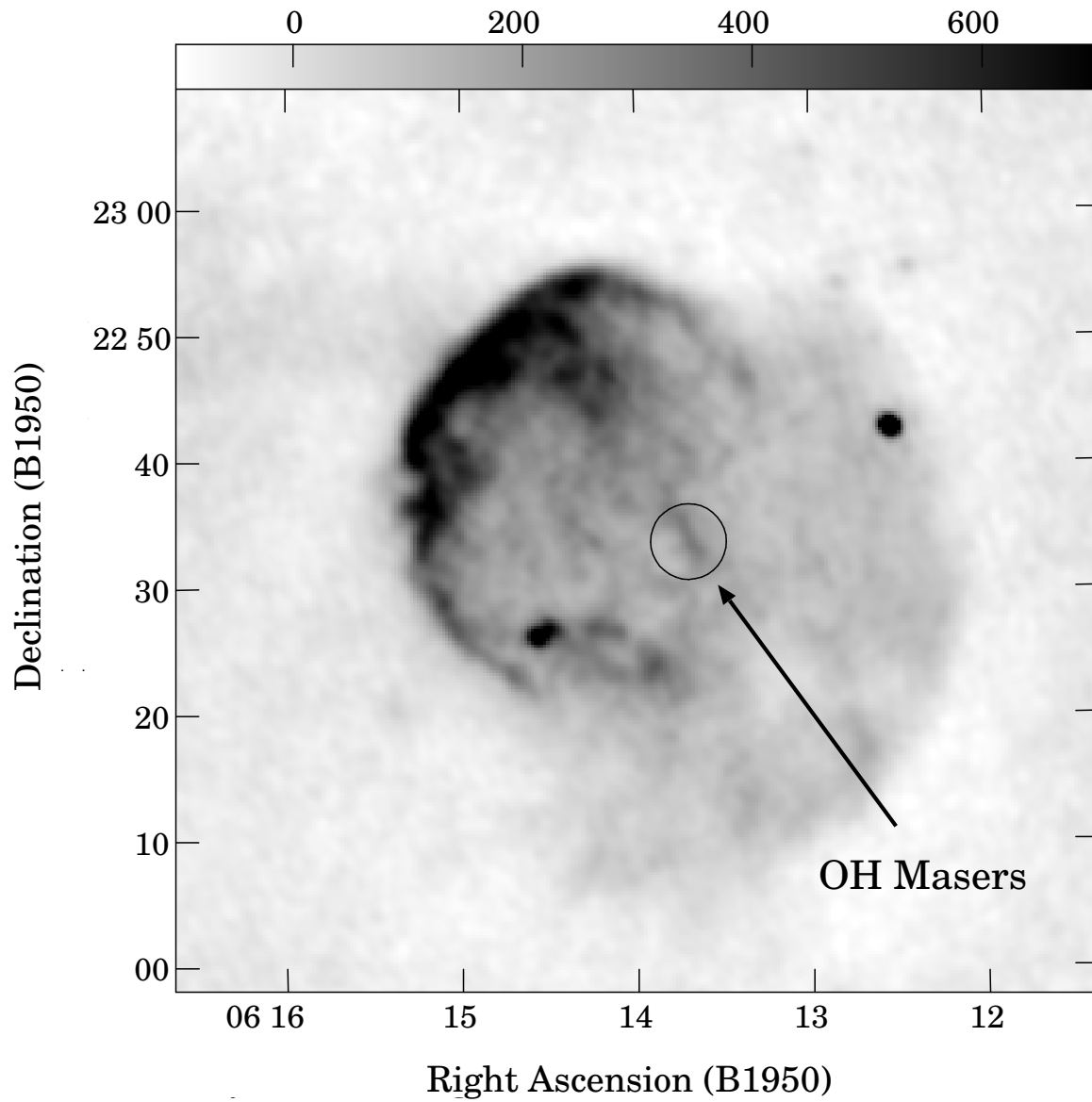
W44 SNR with OH Masers

1442 MHz Continuum Grey Scale in mJy/beam

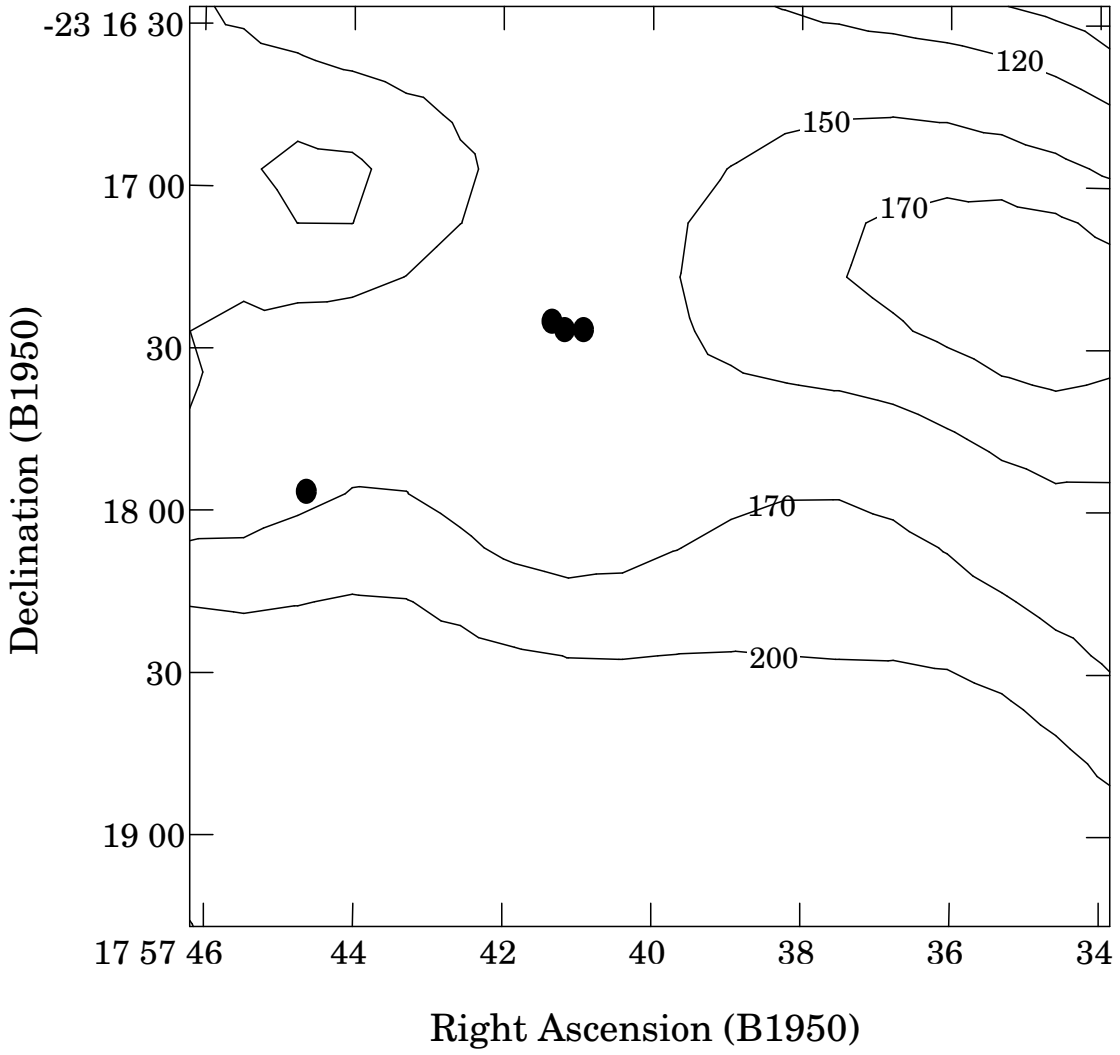


IC443 SNR with OH Masers

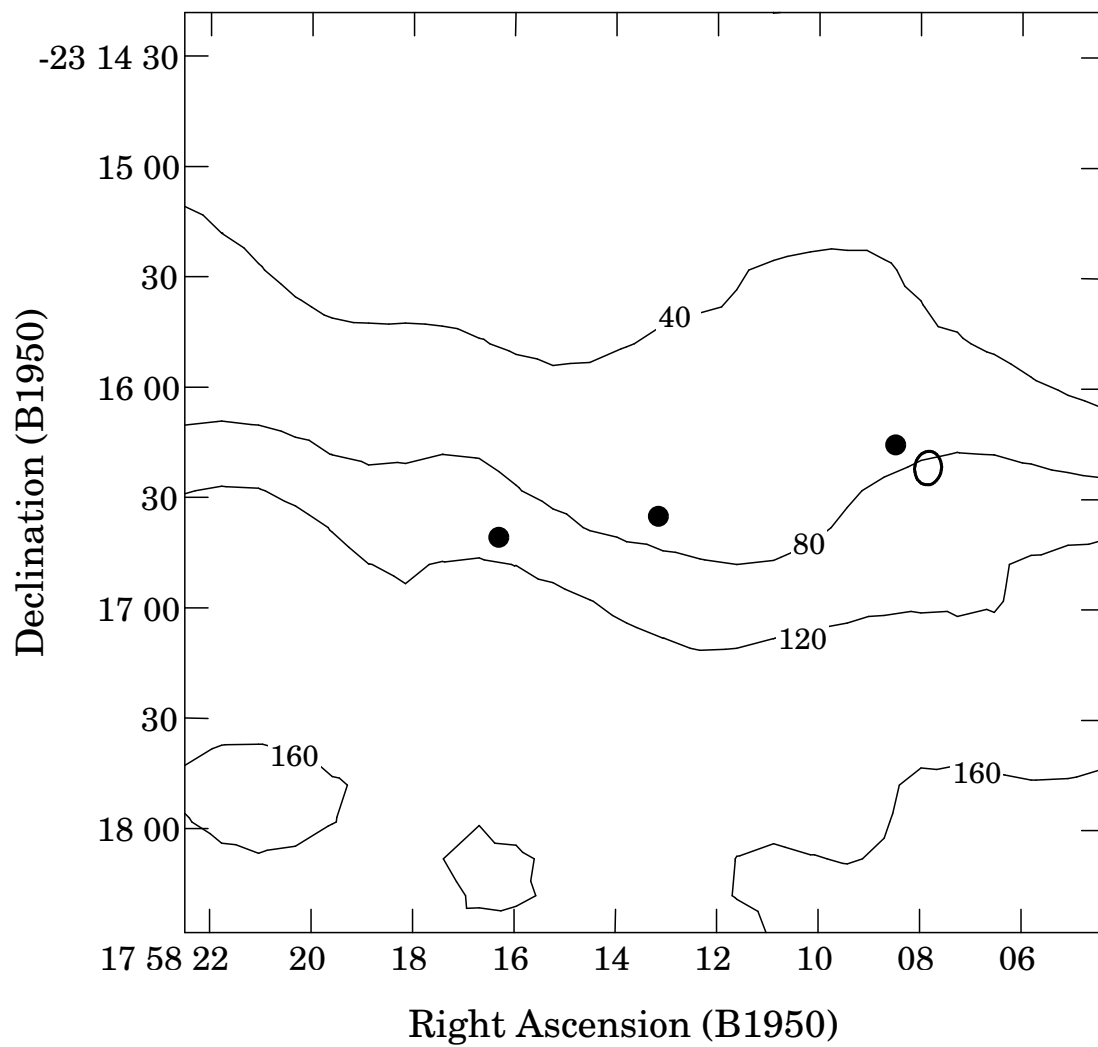
330 MHz Continuum Grey Scale in mJy/beam



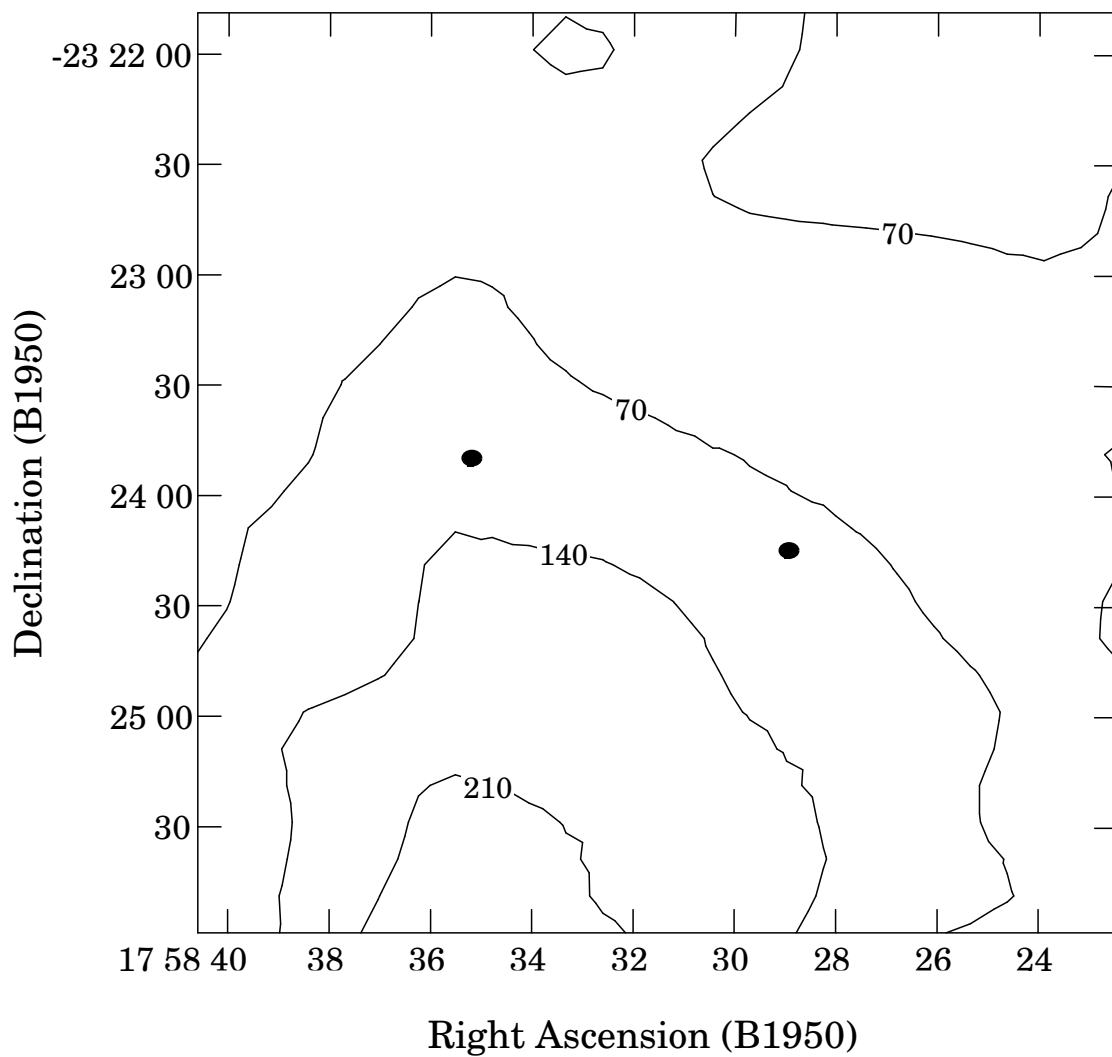
W28 OH Region A



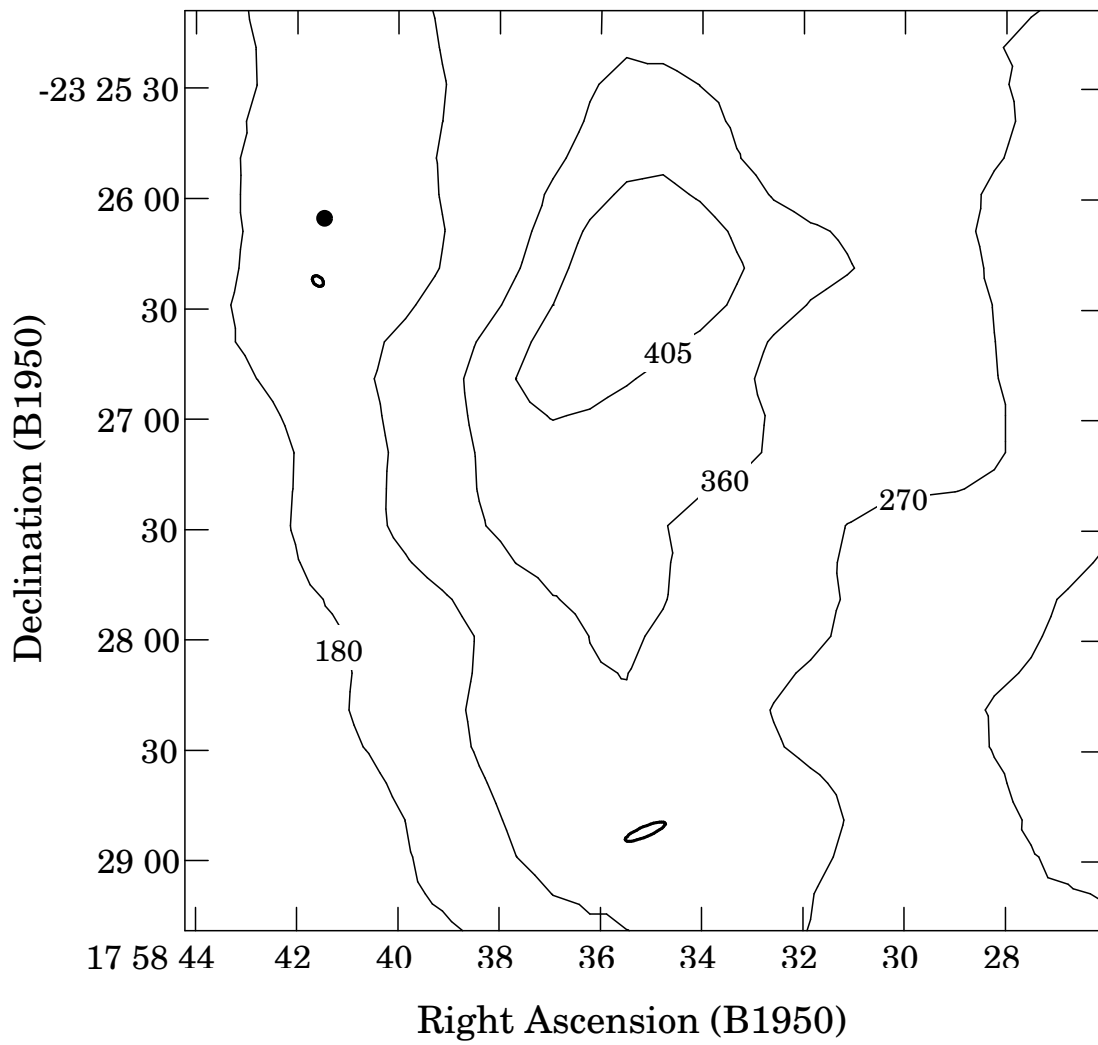
W28 OH Region B



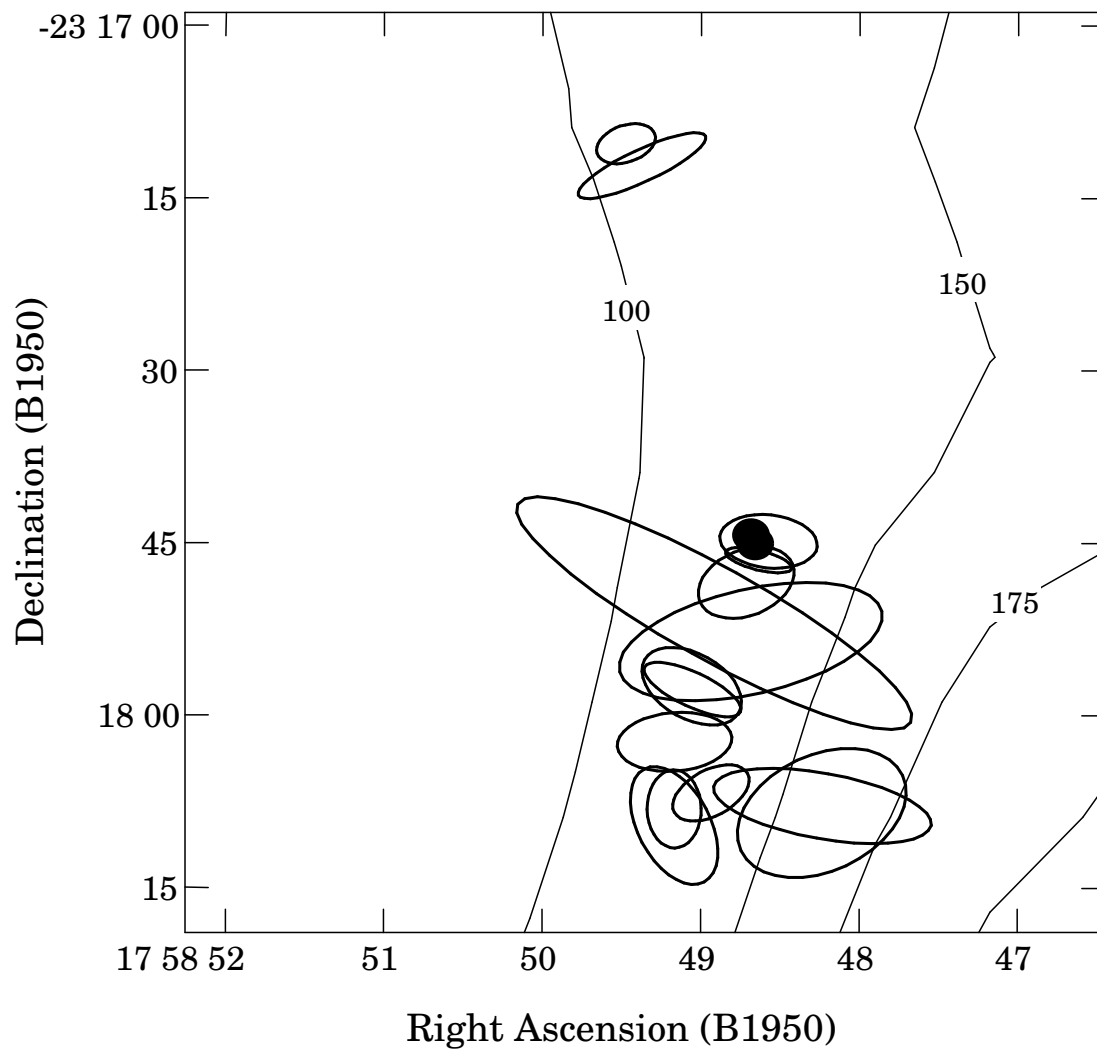
W28 OH Region C



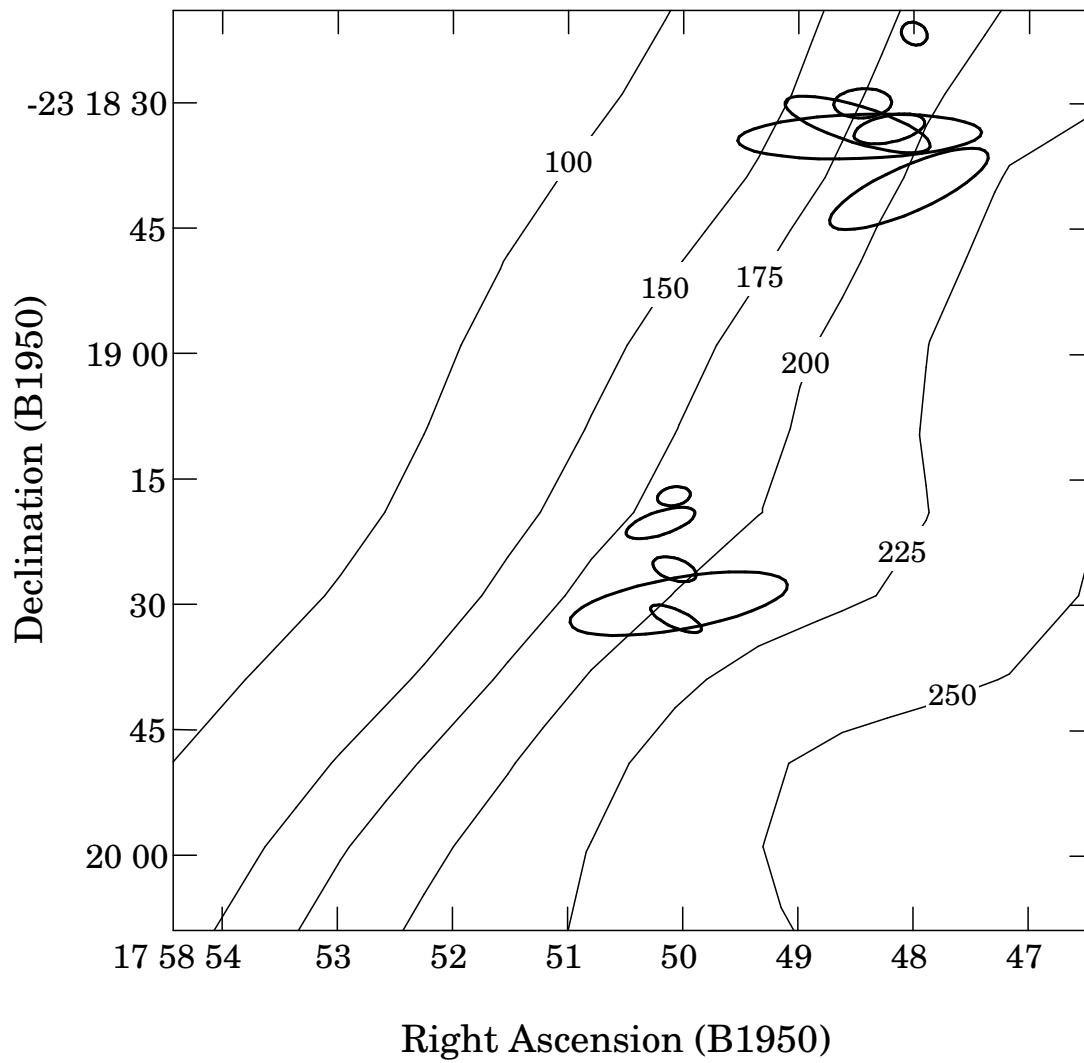
W28 OH Region D



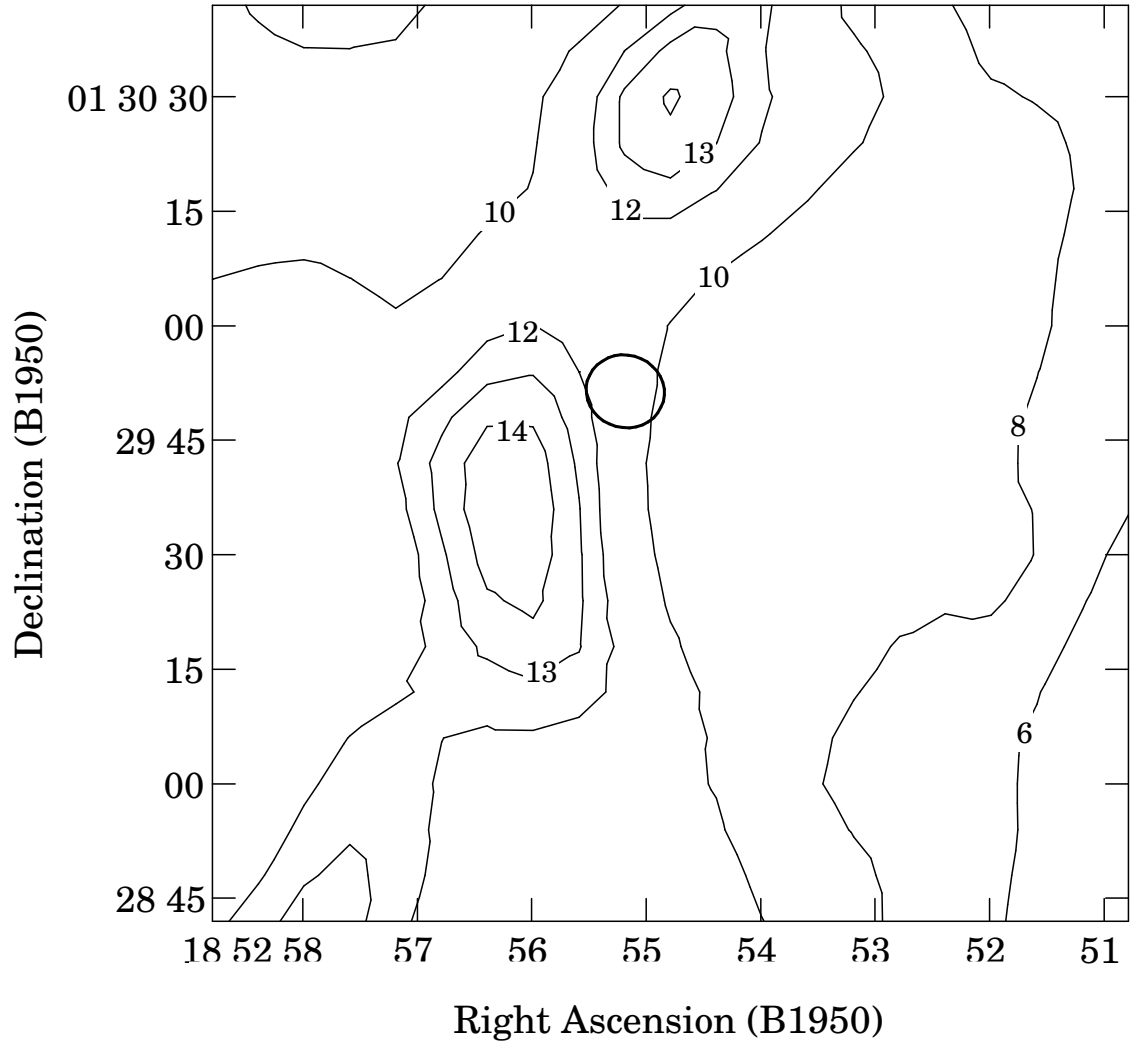
W28 OH Region E



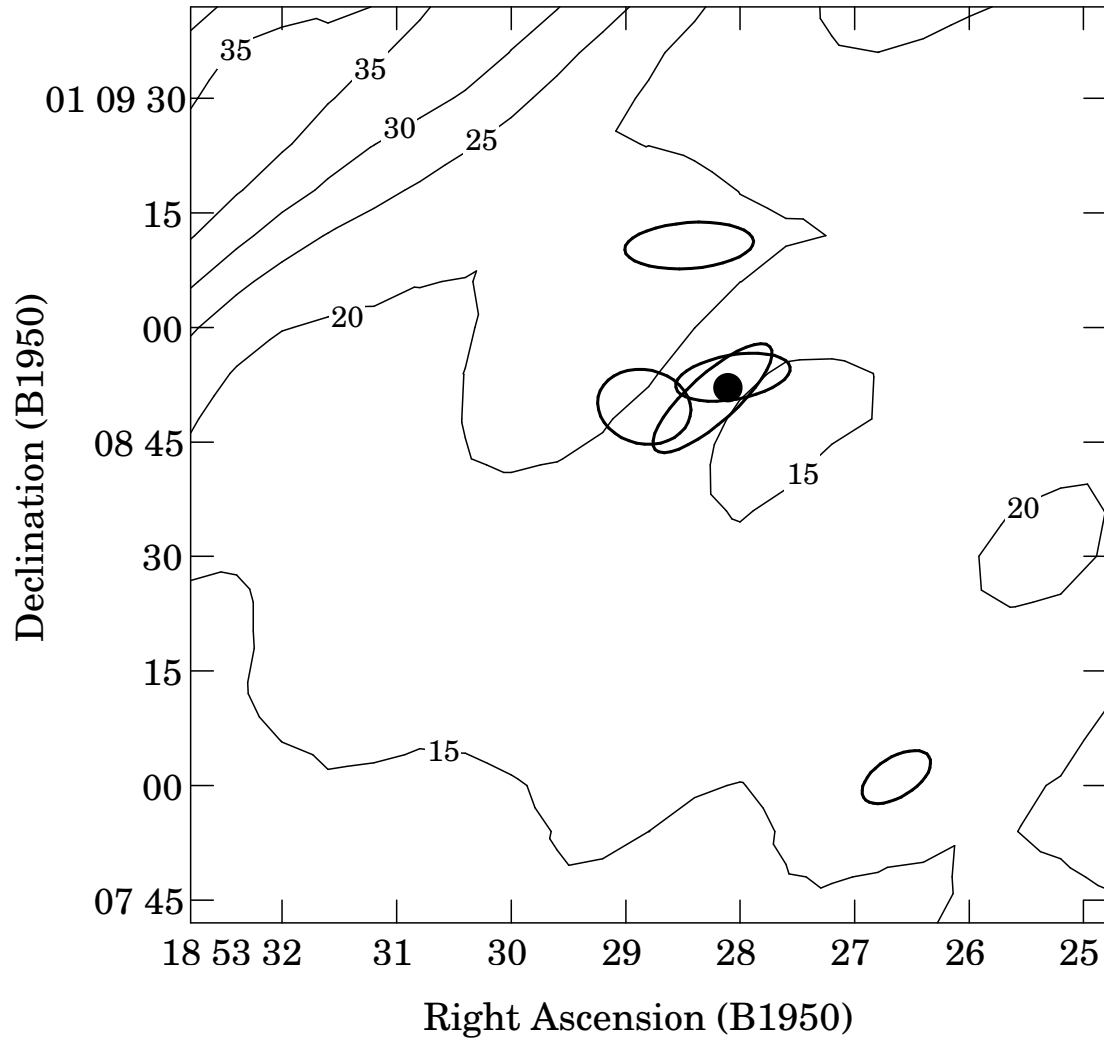
W28 OH Region F



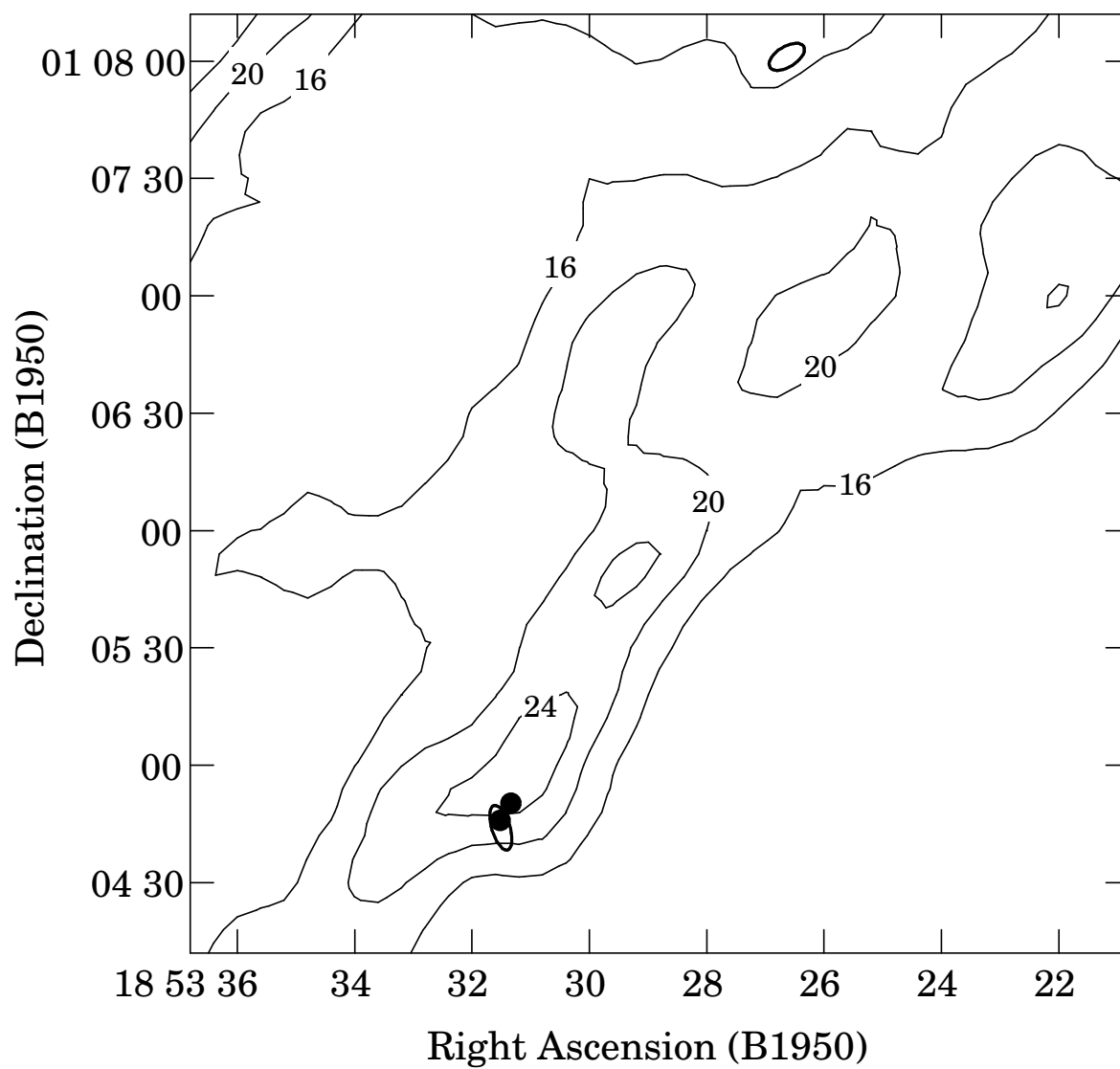
W44 OH Region A



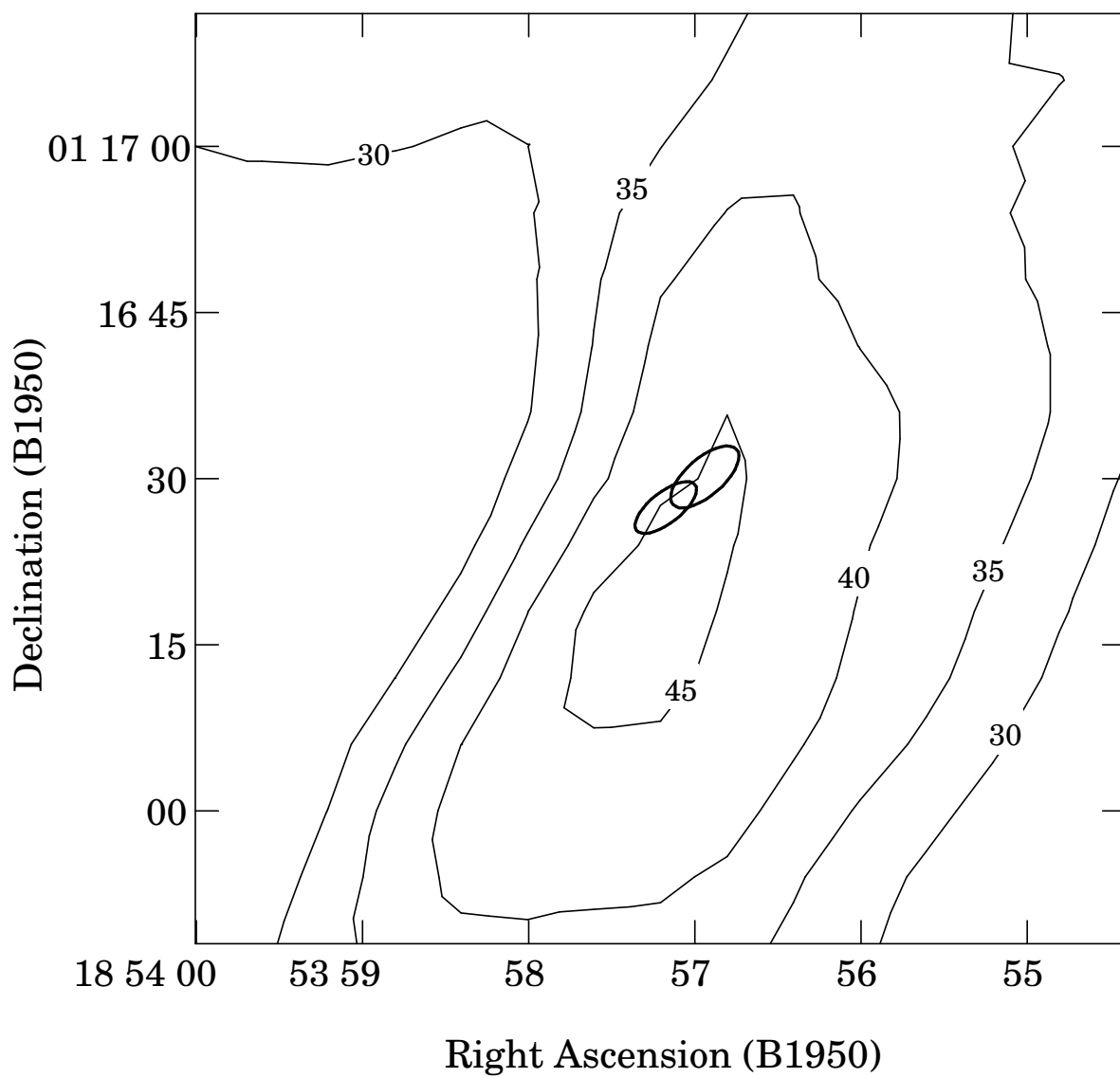
W44 OH Region B



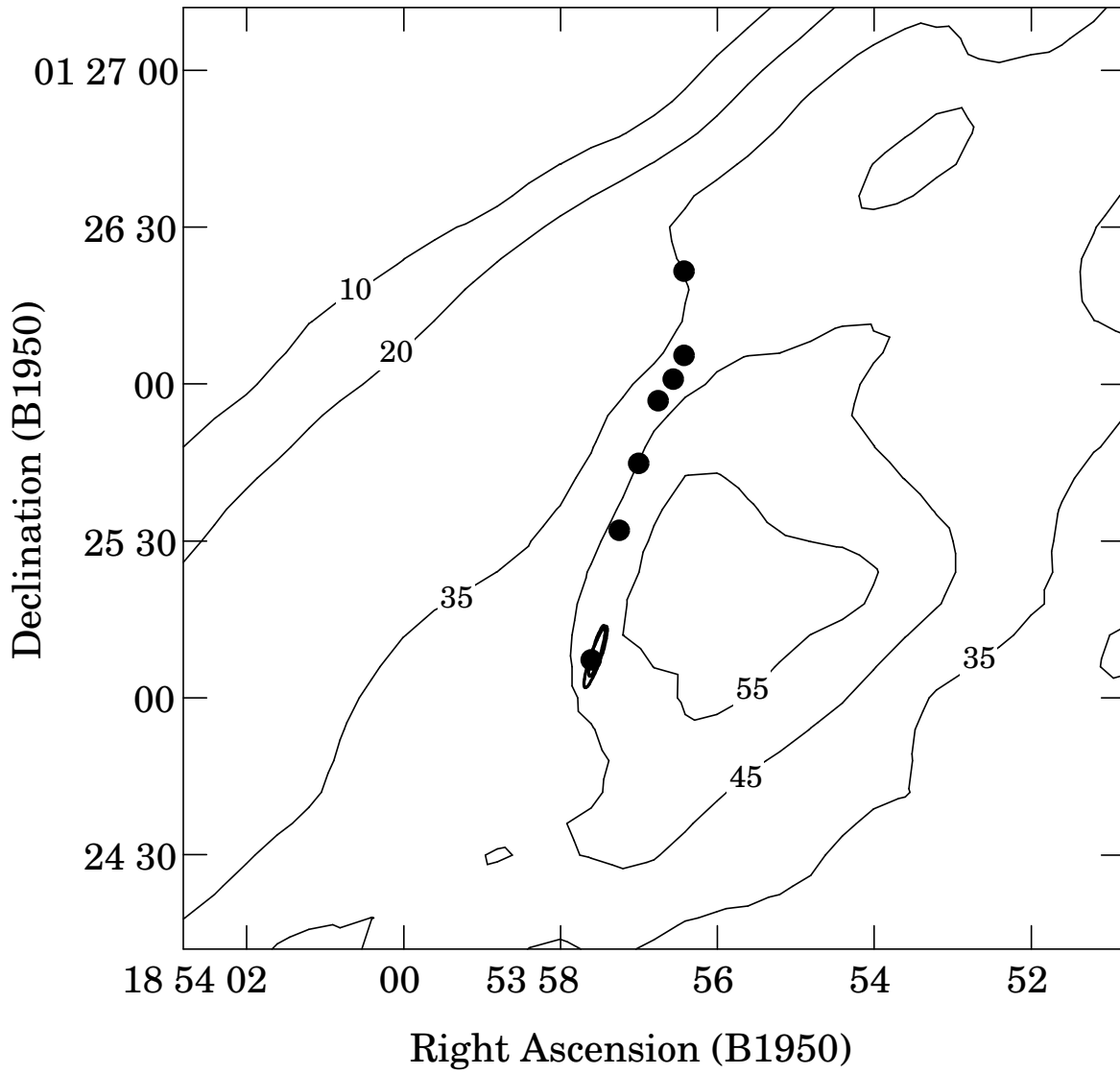
W44 OH Region C



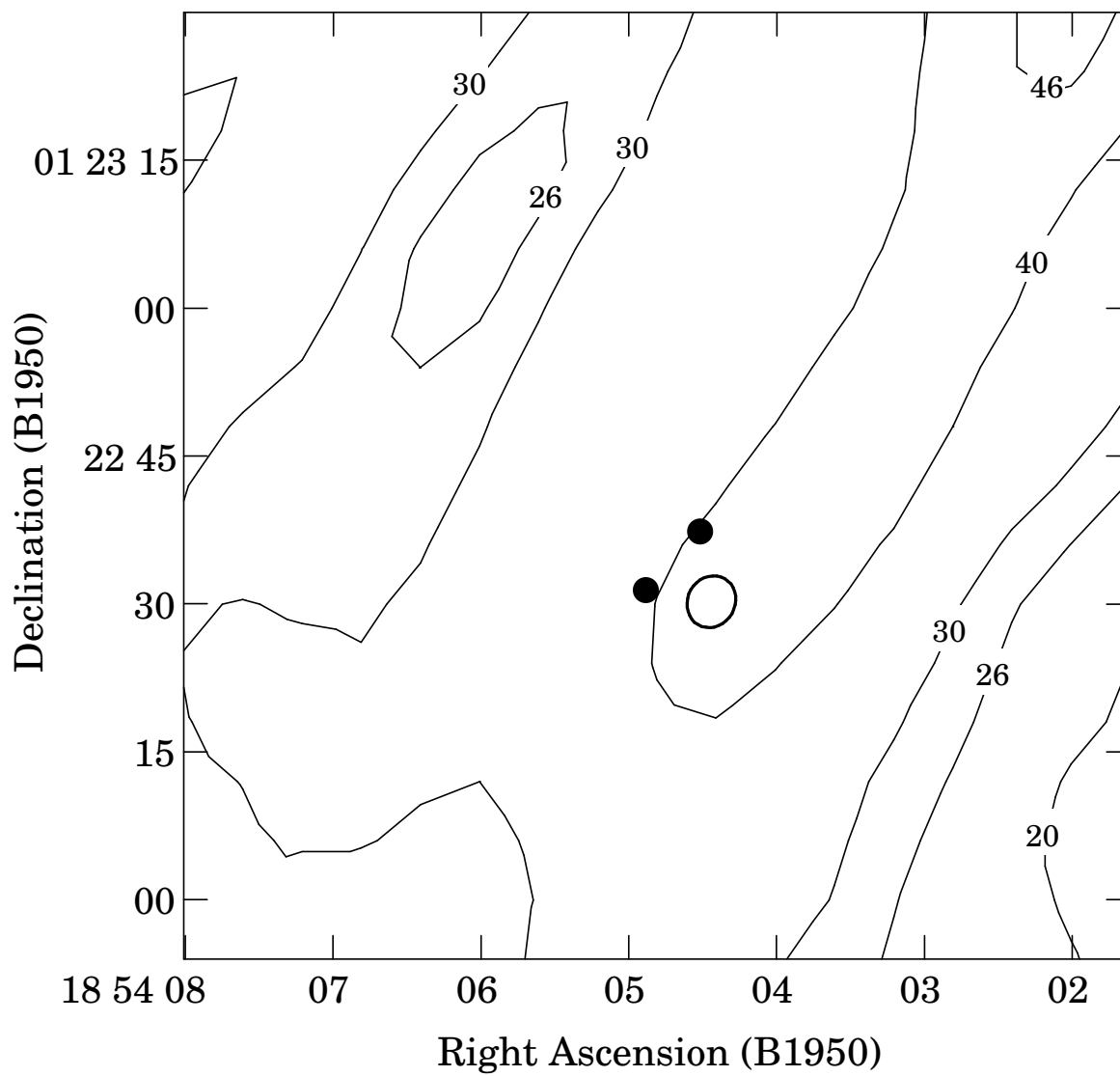
W44 OH Region D



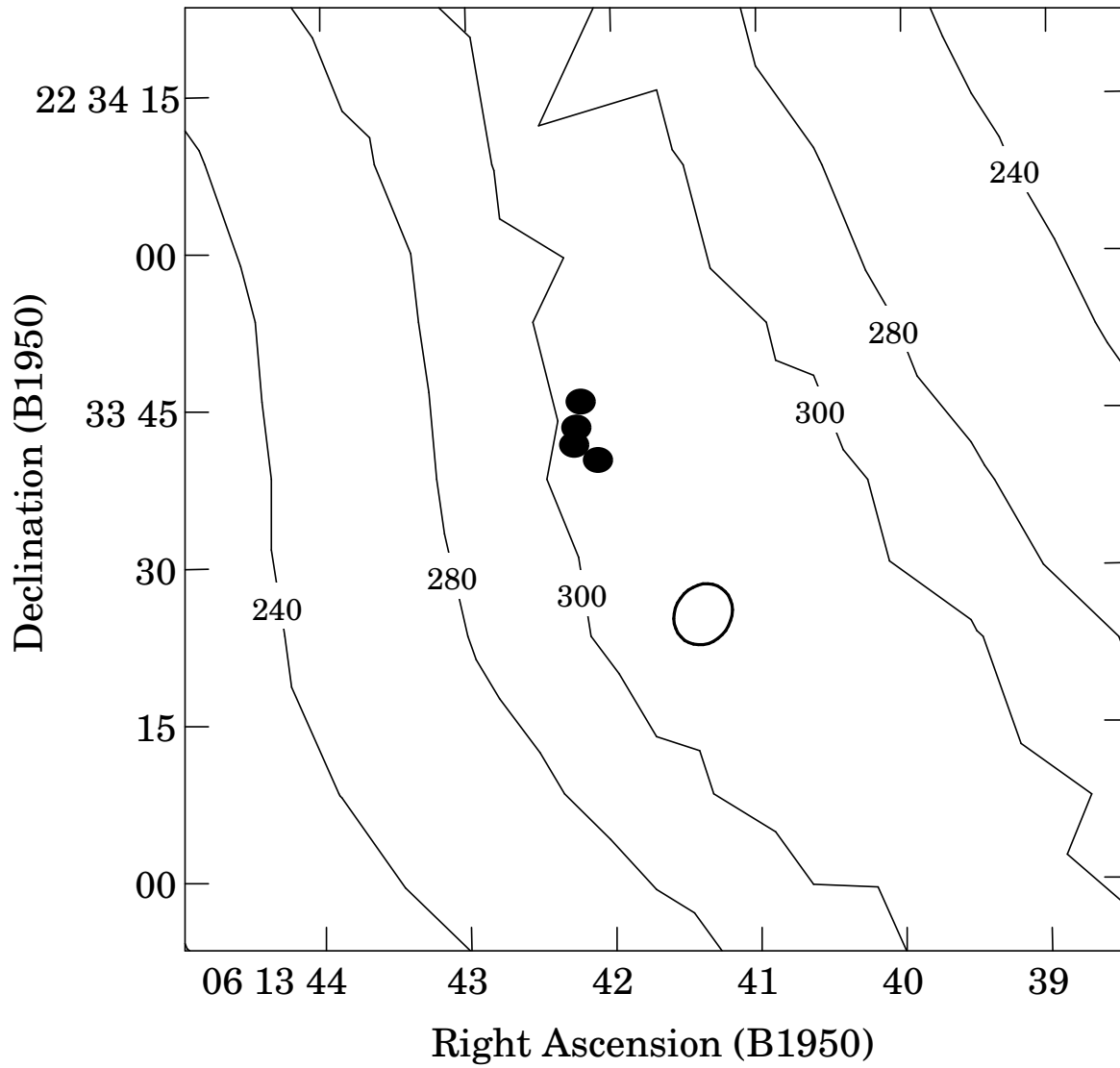
W44 OH Region E

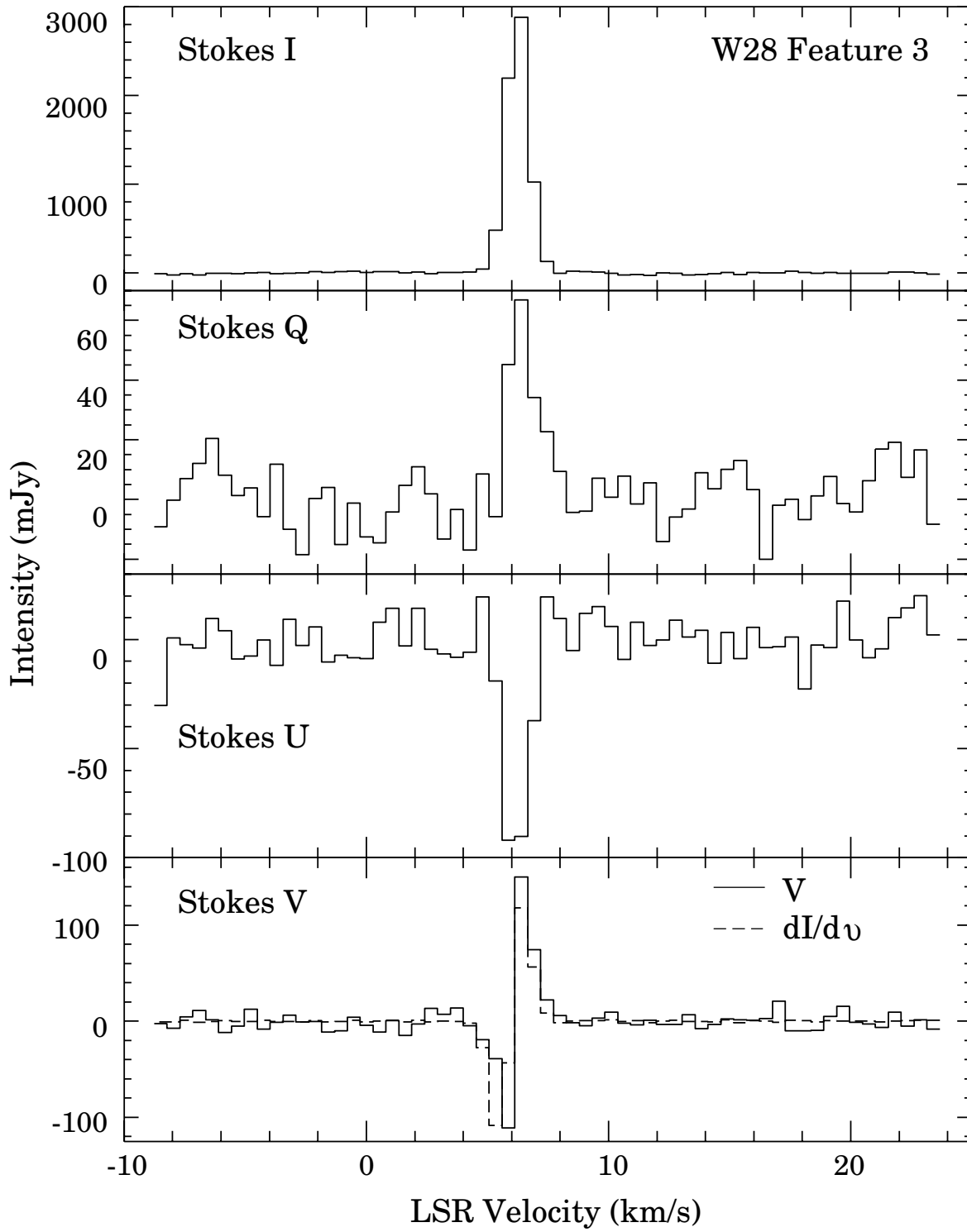


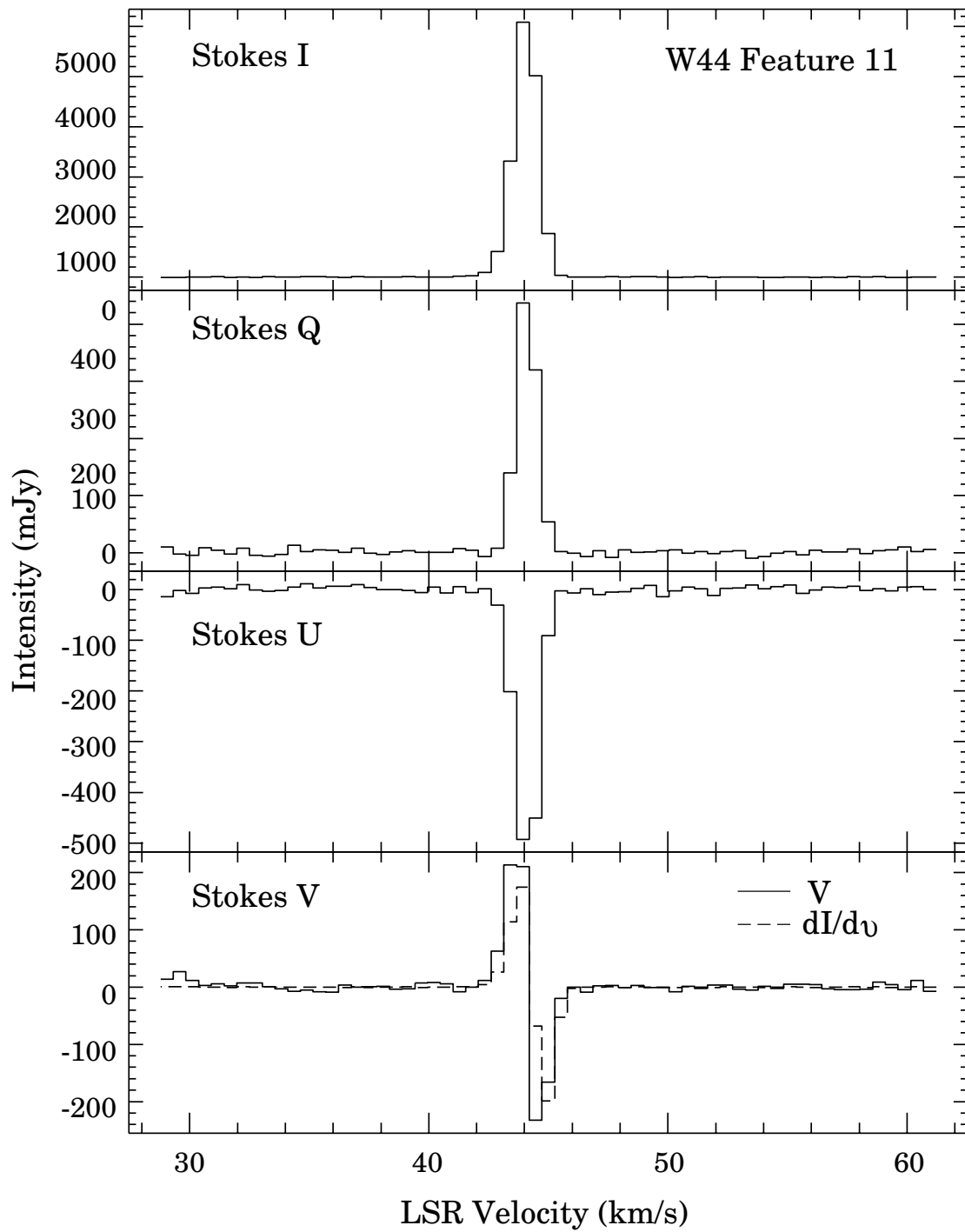
W44 OH Region F



IC 443 OH Region







This figure "fig10.jpg" is available in "jpg" format from:

<http://arxiv.org/ps/astro-ph/9706067v1>

TABLE 1
OBSERVATIONAL SUMMARY

Source	Right Ascension (B1950)	Declination (B1950)	v_{LSR} (km s^{-1})	Beam ($''$)	$\sigma_{\text{rms}}/\text{Channel}$ (mJy beam^{-1})
W 28	$17^{\text{h}} 58^{\text{m}} 01^{\text{s}}.0$	$-23^{\circ} 16' 02''.5$	7.46	1.9 x 1.0	15
	$17^{\text{h}} 58^{\text{m}} 48^{\text{s}}.9$	$-23^{\circ} 18' 00''.0$	11.76		
	$17^{\text{h}} 58^{\text{m}} 41^{\text{s}}.5$	$-23^{\circ} 26' 24''.0$	14.13		
W 44	$18^{\text{h}} 53^{\text{m}} 59^{\text{s}}.0$	$01^{\circ} 23' 54''.0$	45.00	1.2 x 1.1	10
IC 443	$06^{\text{h}} 13^{\text{m}} 42^{\text{s}}.1$	$22^{\circ} 33' 42''.0$	-4.60	1.1 x 0.9	5

TABLE 2
 FITTED PARAMETERS OF 1720 MHz OH MASERS TOWARD W28

Feature	Region ^a	Right Ascension (B1950)	Declination (B1950)	S_{peak} (mJy bm^{-1})	v_{LSR} (km s^{-1})	Δv^b (km s^{-1})	θ_{max} ($''$)	θ_{min} ($''$)	P.A. ^c (degrees)
1	A	17 ^h 57 ^m 40 ^s .892	-23° 17' 26'' 20	580	4.81	—	—	—	—
2	A	41.125	26.11	1095	4.81	—	—	—	—
3	A	41.304	24.78	2875	6.30	—	—	—	—
4	A	44.604	56.68	120	5.81	2.39	—	—	—
5	B	58 07.851	16 21.55	195	5.34	—	0.92	0.73	172
6	B	08.401	15.63	530	5.34	—	—	—	—
7	B	13.110	34.83	1075	5.67	1.42	—	—	—
8	B	16.230	41.21	120	6.25	2.19	—	—	—
9	C	28.878	24 15.41	115	7.77	—	—	—	—
10	D	35.114	28 51.89	930	7.36	2.62	1.18	0.28	113
11	C	35.148	23 50.61	605	7.24	—	—	—	—
12	D	41.414	26 05.33	355	13.49	1.37	—	—	—
13	D	41.596	22.39	2830	14.08	1.03	0.34	0.24	49
14	F	47.999	18 21.64	3575	15.24	2.69	0.32	0.26	63
15	F	48.044	40.22	195	12.29	—	2.06	0.55	114
16	F	48.215	33.03	1040	12.29	—	0.86	0.32	102
17	E	48.231	07.86	190	12.29	—	1.92	0.57	80
18	E	48.236	08.47	130	13.89	—	1.55	1.01	115
19	F	48.446	29.97	1645	11.23	—	0.69	0.35	93
20	F	48.472	33.94	5025	9.70	1.94	2.92	0.53	92
21	F	48.490	32.50	5875	10.29	0.65	1.81	0.44	73
22	E	48.573	17 44.85	5185	15.18	1.50	0.85	0.46	84
23	E	48.635	46.49	1620	15.94	1.20	0.59	0.17	76
24	E	48.647	44.37	10160	13.29	1.08	—	—	—
25	E	48.675	44.01	220	14.41	—	—	—	—
26	E	48.685	53.57	520	11.23	—	2.34	0.91	103
27	E	48.714	48.45	1200	12.82	—	0.87	0.57	112
28	E	48.915	51.11	115	10.70	—	3.91	0.80	61
29	E	48.935	18 06.74	525	12.74	4.62	0.72	0.40	118
30	E	49.051	17 57.75	24420	11.72	1.09	0.92	0.30	65
31	E	49.057	57.46	12550	11.97	0.59	0.94	0.57	61
32	E	49.165	18 02.30	2555	10.40	1.21	1.00	0.51	95
33	E	49.167	09.58	7090	9.75	1.60	1.11	0.63	28
34	E	49.167	08.13	2950	11.40	1.29	0.68	0.47	1
35	E	49.375	17 12.18	1560	11.89	1.28	1.22	0.28	115
36	E	49.476	10.27	7910	11.47	1.10	0.53	0.32	109
37	F	50.038	19 29.85	490	10.39	2.77	2.64	0.62	100
38	F	50.061	31.66	210	8.58	—	0.66	0.21	66
39	F	50.074	25.74	73035	11.66	0.59	0.54	0.26	72
40	F	50.081	17.00	1685	9.11	—	0.40	0.22	100
41	F	50.196	20.21	4440	10.06	1.00	0.86	0.28	108

^aThe region names are for reference to Figure 1.

^b“—” entries imply that a maser feature was seen in three or fewer channels.

^c θ_{max} , θ_{min} , and P.A. are the angular sizes and position angle of the feature in the peak channel; “—” entries imply that the feature was unresolved at the resolution of the observations.

TABLE 3
 FITTED PARAMETERS OF 1720 MHz OH MASERS TOWARD W44

Feature	Region ^a	Right Ascension (B1950)	Declination (B1950)	S_{peak} (mJy bm^{-1})	v_{LSR} (km s^{-1})	Δv^b (km s^{-1})	θ_{max} ($''$)	θ_{min} ($''$)	P.A. ^c (degrees)
1	A	18 ^h 52 ^m 55 ^s .182	01° 29' 51".41	960	42.68	1.26	1.03	0.95	75
2	B	53 26.636	08 01.11	220	45.53	—	1.01	0.52	122
3	B	28.064	53.48	300	45.53	—	1.52	0.58	100
4	B	28.069	52.15	60	45.00	—	—	—	—
5	B	28.241	50.75	90	45.53	—	2.02	0.63	132
6	B	28.445	09 10.74	160	45.00	—	1.69	0.60	94
7	B	28.838	08 49.62	1290	44.65	0.85	1.23	0.97	78
8	C	31.275	04 49.61	700	46.13	1.12	—	—	—
9	C	31.495	45.44	40	45.53	—	—	—	—
10	C	31.507	44.05	60	46.59	—	1.19	0.46	17
11	E	54.596	25 19.19	6640	44.09	1.18	0.89	0.18	137
12	E	56.386	26 21.50	80	45.00	—	—	—	—
13	E	56.388	05.04	50	45.00	—	—	—	—
14	E	56.533	00.76	110	45.53	—	—	—	—
15	E	56.703	25 56.65	40	45.00	—	—	—	—
16	D	56.940	16 30.15	490	43.94	—	0.76	0.34	131
17	E	56.966	25 44.22	120	44.47	—	—	—	—
18	D	57.175	16 27.39	2460	43.94	—	0.67	0.28	128
19	E	57.204	25 31.52	90	45.00	—	—	—	—
20	E	57.537	08.99	5460	44.28	1.19	1.01	0.16	164
21	E	57.551	07.86	780	43.67	1.53	1.24	0.20	161
22	E	57.575	06.90	1000	43.94	—	—	—	—
23	F	54 04.442	22 30.23	3890	46.81	1.10	0.54	0.48	150
24	F	04.489	37.46	8940	46.91	0.79	—	—	—
25	F	04.856	31.51	80	46.06	—	—	—	—

^aThe region names are for reference to Figure 2.

^b“—” entries imply that a maser feature was seen in three or fewer channels.

^c θ_{max} , θ_{min} , and P.A. are the angular sizes and position angle of the feature in the peak channel; “—” entries imply that the feature was unresolved at the resolution of the observations.

TABLE 4
 FITTED PARAMETERS OF 1720 MHz OH MASERS TOWARD IC 443

Feature	Right Ascension (B1950)	Declination (B1950)	S_{peak} (mJy bm^{-1})	v_{LSR} (km s^{-1})	Δv^a (km s^{-1})	θ_{max} ($"$)	θ_{min} ($"$)	P.A. ^b (degrees)
1	06 ^h 13 ^m 42 ^s .219	22° 33' 43'' 41	3890	-4.64	0.61	—	—	—
2	42.247	42.14	205	-4.60	—	—	—	—
3	42.192	45.79	365	-4.60	—	—	—	—
4	41.390	25.38	45	-4.07	—	0.53	0.61	54
5	42.077	40.09	125	-4.60	—	—	—	—
6	42.223	43.19	65	-5.13	—	—	—	—

^a“—” entries imply that a maser feature was seen in three or fewer channels

^b θ_{max} , θ_{min} , and P.A. are the angular sizes and position angle of the feature in the peak channel; “—” entries imply that the feature was unresolved at the resolution of the observations.

TABLE 5
POLARIZATION PROPERTIES OF OH MASERS

Feature	V_{peak} (mJy bm^{-1})	Q_{peak} (mJy bm^{-1})	U_{peak} (mJy bm^{-1})	P_l %	χ deg	B_{\parallel} (milliGauss)
W28 2	S	-60	-30	6.7	32	$+0.34 \pm 0.20$
3	S	+60	-90	3.2	-14	$+0.30 \pm 0.08$
7	-15	+30:	+33:	3.8	22	
14	complex					
15	-15	—	—			
16	S	—	+60	5.3		$+0.34 \pm 0.08$
17	—	+15:	—	8.4		
18	-30:	+15:	—	12.3		
19	+45	—	—			
20		+75	-120	2.7	-29	
21	S	-70	-60	1.6	24	$+0.25 \pm 0.04$
22	complex	—	+75	1.5		
23	S	—	—			$+0.18 \pm 0.08$
24	S	-180	+150	2.4	-25	$+0.31 \pm 0.03$
27	S	—	—			$+0.45 \pm 0.25$
28	-90	—	—			
29	+45	—	—			
30	S	-75	+60	0.4	-25	$+0.11 \pm 0.03$
31	S	-90	+75	0.9	-25	$+0.10 \pm 0.02$
32	complex	—	+45	1.5		
33	+60	-30	+75	1.1	-13	
34	S	—	+60	1.8		$+0.11 \pm 0.03$
35	-45	—	—			
36	S	+30:	+30:	0.5	22	$+0.09 \pm 0.03$
37	—	—	-30	6.1		
38	—	-45:	-15:	20.9	30	
39	complex	complex	complex			
40	—	+45	-45	3.7	-26	
41	—	+30	-90	2.1	-34	
W44 1	+60	-60	-80	10.3	21	
7	-100	-20:	+70	5.7	-10	
8	-60	-30	-70	10.6	13	
11	S	+440	-490	9.9	-24	-0.28 ± 0.09
16	-20	—	—			
18	-110	—	+170	6.7		
20	S	+300	-400	9.2	-27	-0.23 ± 0.09
21	-30	+50	-110	15.2	-34	
22	-60	+110	-190	22.0	-31	
23	S	-320	-20	8.2	43	-0.30 ± 0.07
24	S	+260	-320	4.6	-26	-0.12 ± 0.03
IC 443 1	+275	-110	-125	4.2	21	

NOTE.—In the V column, S means that the profile had an S shape; thus we can estimate the magnetic field. The fields in the B_{los} column are computed using the thermal relationship, thus these are upper limits to the magnetic field. The colons mean that the fluxes are uncertain and near the detection limit; “complex” means that the spectra are complex and likely to be the superposition of two or more spectral or spatial components. The errors on the magnitude of the field are almost always dominated by the goodness of fitting the V profile to the I derivative profile.